Medizinische Fakultät
der
Universität Duisburg-Essen

Aus dem Institut für Immunologie

The generation and characterization of a beneficial anti-tumoral Lymphocytic choriomeningitis virus strain

I n a u g u r a l - D i s s e r t a t i o n
zur
Erlangung des Doktorgrades der Medizin
durch die Medizinische Fakultät
der Universität Duisburg-Essen

Vorgelegt von
Michael Bergerhausen
aus Marl
2023

DOI: 10.17185/duepublico/81775
URN: urn:nbn:de:hbz:465-20240403-091823-2

Dekan: Herr Univ.-Prof. Dr. med. J. Buer
1. Gutachter: Herr Univ.-Prof. Dr. med. K. S. Lang
2. Gutachter: Frau Priv.-Doz. Dr. rer. nat. K. Sutter
3. Gutachter: Herr Univ.-Prof. Dr. rer. nat. St. Ludwig

Tag der mündlichen Prüfung: 26. Februar 2024

Content

1. Introduction 6

1.1 Lymphocytic Choriomeningitis Virus 6

1.1.1 Viral Structure 6

1.1.2 Viral Entry 7

1.1.3 Replication Cycle 8

1.2 Virus Passage 9

1.2.1 Fast Evolution Platform 10

1.3 Immune System 10

1.3.1 Cells of the Innate Immune System 11

1.3.2 Pattern Recognition Receptors 12

1.3.3 Type I Interferon 13

1.3.4 Antigen Presentation via Major Histocompatibility Complex 13

13.5 Adaptive Immune System 13

1.3.6 T cells 14

1.3.7 Antibodies 14

1.4 Immune Response against LCMV 15

1.4.1 Innate Response 16

1.4.2 Adaptive Response 16

1.5 *In Vivo* Tumor Models 17

1.5.1 Syngeneic Models 17

1.5.2 Xenograft Models 18

1.6 Current Virotherapeutical Approaches 18

1.7 Aim of this Work 19

2. Materials and Methods 21

2.1 Materials 21

2.1.1 Media / Buffers 21

2.1.2 Reagents 22

2.2 Methods 25
2.2.1 Cells 26
2.2.3 Viruses 27
2.2.4 Virus Sequencing 30
2.2.5 RT-qPCR 32
2.2.6 Mice 33
2.2.7 *Ex Vivo* Analysis of T cells 36
2.2.8 Flow Cytometry 37
2.2.9 Immunofluorescence Imaging 37
2.2.10 IFNα ELISA 38
2.2.11 Measurement of LDH, ALAT and ASAT 38
2.2.12 Statistical analysis 38
2.3 Software 38
2.4 Hardware 39
2.4.1 Devices 39
2.4.2 Manual tools 39
3. Results 40
3.1 Passage of LCMV-WE in H1975 Cells 40
3.2 3D-structure of mutated LCMV-GP 41
3.3 Generation of Single-Mutant Viruses 43
3.4 *In Vitro* Replication of Mutant Viruses 45
3.5 *In Vivo* Replication of LCMV-P52 47
3.6 Innate Immune Response 49
3.6.1 IFN-I 49
3.6.2 TLR2 50
3.7 Adaptive Immune Response 52
3.7.1 $CD8^+$ T cells 52
3.7.2 Development of Memory T Cells 53

3.7.3 Neutralizing Antibody Response 54
3.8 Virus-Induced Hepatitis 54
3.9 Tumor Growth Inhibition by Mutant Viruses 55
3.10 Combination Therapy with PD-1 Blockade 56
4. Discussion 58
4.1 Proof of Principle 58
4.2 Differences of WE and Mutant P52 58
4.2.1 *In Vitro* Replication 59
4.2.2 *In vivo* Replication 60
4.2.3 Innate Immune Response 60
2.2.4 Adaptive Immune Response 61
2.2.5 Immunopathology 62
2.2.6 Tumor Growth Inhibition 63
4.3 Possible Mode of Action 63
4.4 Limitations of this Work 64
4.5 Outlook 65
5. Conclusion 67
6. Literature 68
7. Appendix 77
7.1 List of Figures 77
7.2 List of Tables 78
7.3 Abbreviations 79
8. Lebenslauf 82

1. Introduction

1.1 Lymphocytic Choriomeningitis Virus

The Lymphocytic Choriomeningitis Virus (LCMV) belongs to the family of Arenaviruses, which can be divided into two distinct classes depending on their natural occurrence. The New-World arenaviruses are mainly found in rodents in South America where they cause around 1,000 human infections per year with a mortality of 15 - 30 %. Introduction of a vaccine against the Junín virus (JUNV) reduced the number drastically (McLay et al., 2014). On the other side, the Old-World arenaviruses are found in Africa where one of them, the Lassa Virus (LASV), causes endemic outbreaks in Western Africa with 100,000 - 300,000 cases and 5,000 deaths every year (Coyle, 2016).

Within this group, the LCMV is not known to cause severe disease in healthy humans. 5 % of the human population have antibodies detectable in the serum (Peters, 2006), indicating an previous infection without the need for special medical treatment. Acquired infections often come with mild symptoms including fever, headache and fatigue, reflecting a flu-like infection, but may also cause aseptic meningitis with full recovery in most of the cases (Bonthius, 2012). Fatal cases of LCMV infection are only known in the context of organ-transplantation. This indicates the importance of immune activation and response during LCMV infection, which is inhibited during strong immunosuppression after organ-transplantation (Macneil et al., 2012).

Additionally, LCMV is one of the best studied viruses in regarding the immune response in their natural host, the house mouse *Mus musculus*.

1.1.1 Viral Structure

Like all arenaviruses, the LCMV is an enveloped virus with a bi-segmented ambisense ribonucleic acid (RNA) genome (Hallam et al., 2018). The smaller S-segment codes for the glycoprotein complex (GPc) and the nucleoprotein (NP), whereas the larger L-segment codes for the polymerase L and the matrix-protein Z.

The GPc is post-translationally cleaved into the stable signaling peptide (SSP), the glycoprotein subunit 1 (GP1) and the glycoprotein subunit 2 (GP2). The GP1 binds to the cellular receptor, whereas the GP2 contains a fusion peptide, mediating the pH-dependent fusion with the endosomal membrane (Di Simone et al., 1994).

The NP is associated to the RNA and together with the polymerase L, it forms the ribonucleoprotein (RNP) complex, that performs the main steps of transcription and replication.

Last, the small Z protein mediates the budding of new virions (Hallam et al., 2018). The structure of the virion is visualized in Figure 1.

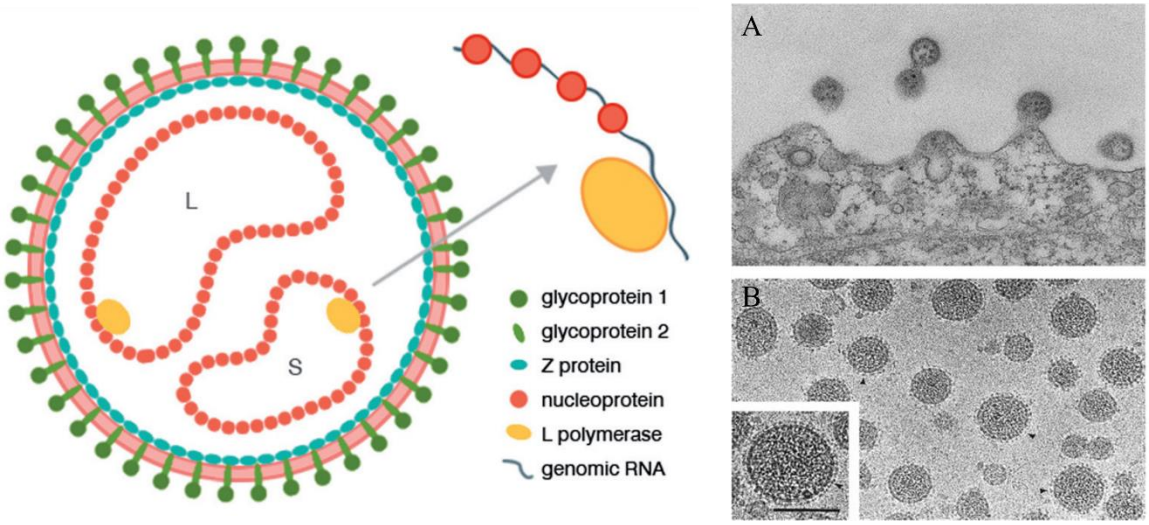

Figure 1: LCMV structure. Left: schematic assembly of LCMV virion taken from Lapošová et al. (2013). Right: electron microscopy of LCMV virions budding from infected BHK-21 cells (A) and purified virions (B). Arrow heads indicate viral GP, scale bar = 100 nm. Pictures taken form Salvato et al. (2011).

1.1.2 Viral Entry

Arenaviruses enter target cells by receptor-mediated endocytosis. For the Old-World arenavirus LCMV, the reported receptor is the α-Dystroglycan (α-DG), which different strains bind with distinct affinity (Cao et al., 1998; Kunz et al., 2004). This protein mediates the interaction between intracellular actin filaments and extracellular matrix (ECM), making it indispensable for cell adhesion and migration.

After binding to the receptor via GP1, the virus is internalized in an endosome, where the ongoing acidification by fusion with lysosomes triggers the fusion with the late endosomal membrane by GP2 at a pH below 5.8 (Di Simone et al., 1994). The viral RNP is then released into the cytoplasm, where the replication takes place (Figure 2).

Newer studies suggest alternative receptors that can be used by LCMV. This is supported by the finding, that embryonic stem (ES) cells lacking a functional gene for α-Dystroglycan only show slightly decreased replication compared to wildtype ES cells (Kunz et al., 2004). For LASV, the Tyro3 and Axl, but also the Dendritic Cell-Specific Intercellular adhesion molecule-3-Grabbing Non-integrin (DC-SIGN, CD209) and liver and lymph node sinusoidal endothelial calcium-dependent lectin (LSECtin) are described as additional receptors (Shimojima et al., 2012). The close relation between LASV and LCMV, including the use of the same receptor α-DG, suggests a role of these surface molecules for LCMV's binding to target cells.

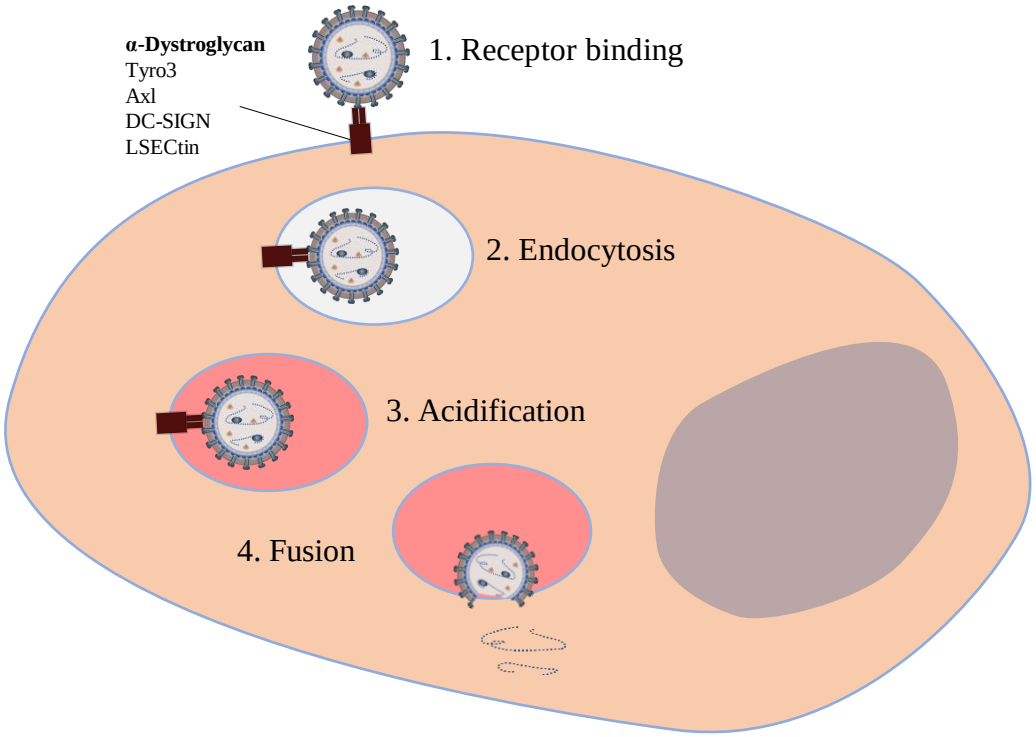

Figure 2: Viral entry. After attachment to the receptor the virus particle is internalized by receptor-mediated endocytosis. Acidification of the late endosome finally triggers the membrane fusion and releases the viral genome into the cytoplasm.

The exact mechanism of receptor binding and membrane fusion is not yet fully understood and needs further investigation.

1.1.3 Replication Cycle

The transcription of the viral genome starts when the viral RNP reaches the cytoplasm. The polymerase and the NP are essential for this process and are therefore produced in the early phase of infection.

Both RNA segments are ambisensed, which means, they contain positive- and negative-sensed RNA within one strand. For arenaviruses, the genes of the NP and polymerase are in negative-sense on the S- and the L-segment, respectively (Hallam et al., 2018). Hence, the viral genome directly serves as a template for the transcription of the two genes, which are indispensable for viral transcription and replication. The 3' untranslated region (3'-UTR) works as a promotor for transcription, while the hairpin structure of the intergenic region (IGR) is terminating it.

In a later stage, the complete genome is transcribed, giving an anti-genomic strand that now serves as a template for the transcription of the initial positive-sensed part of the genome, the genes for GPc and Z. Secondly, the polymerase produces new genome segments with the anti-genome as template (Figure 3).

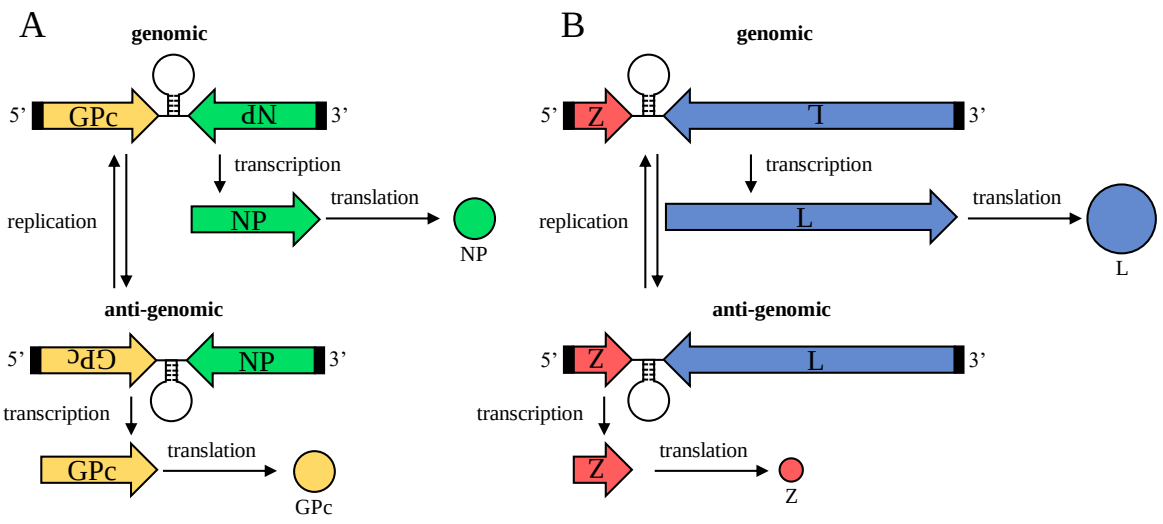

Figure 3: Genome replication and gene transcription. Schematic presentation of S-segment (A) and L-segment (B) RNA replication and transcription. The negative-sense genes, the NP and L, can be transcribed directly from the genomic RNA, for the positive sense genes, the anti-genomic strand serves as template. For the generation of new genomic RNA, the anti-genomic strand is also used as template.

The newly translated glycoprotein complex contains a stable signal peptide (SSP), that directs it into the endoplasmic reticulum (ER), where it is cleaved by site 1 protease (S1P) into GP1 and GP2, and finally transported to the cellular membrane (Kunz et al., 2003).

LCMV is a non-cytopathic virus, which requires a special mechanism to release new virions without lyzing the host cell. This is performed by the matrix-protein Z, which is located at the inner membrane due to a myristoylation. The infectious virions contain the two genomic segments, the polymerase and NP, and the GP at the viral surface. Depending on the host cell and the culture conditions, the majority of released particles is not infectious due to genomic deletions or assembling issues (Weidmann et al., 2011; Ziegler et al., 2016).

1.2 Virus Passage

Serial passaging of viruses in general describes a technique of growing viruses in a certain environment and transferring part of it into a new environment. This can be done *in vitro* on new seeded cells or *in vivo*. This procedure is repeated several times, resulting in a selective pressure on the virus. By that, viruses having an advantage in this environment grow faster and are found predominant to the initial virus.

The new virus is better adapted to the environment, for example the species or the cell line, compared to the initial virus, but is also losing its affinity to the former host. This phenomenon was used by Louis Pasteur to develop a rabies vaccine by passaging rabies virus in rabbits. This led to an adaptation to rabbits by simultaneously reducing the virulence to humans (Smith, 2012). Within the last century, many live-attenuated vaccines were generated by this technique,

including the Modified Vaccinia Virus Ankara (MVA), which was used as a vaccine to eradicate smallpox in Germany in the 1970s (Mayr et al., 1975).

1.2.1 Fast Evolution Platform

According to Charles Darwin, the evolution needs two major aspects, mutagenesis, and selection. The mutagenesis was in this special case done by the lack of proof-reading activity of the viral polymerase. The missing proof-reading included a mismatch every 10^3 to 10^5 bases (Sevilla et al., 2002), meaning statistically at least every tenth virus contained a point mutation.

The selective pressure was reached by repeated infection of tumor cells *in vitro*, bringing up the best tumor-adapted virus.

In contrast to Darwin's theory of evolution which took millions of years, this approach leads to changes in the viral phenotype after a few weeks. Therefore, it was named "Fast Evolution Platform" (FEP).

1.3 Immune System

The immune system of vertebrates is a complex orchestra of many tissues, cellular and non-cellular actors, that protects the host from pathogens, e.g., viruses, but also plays a major role in elimination of malignant cells and tissue regeneration.

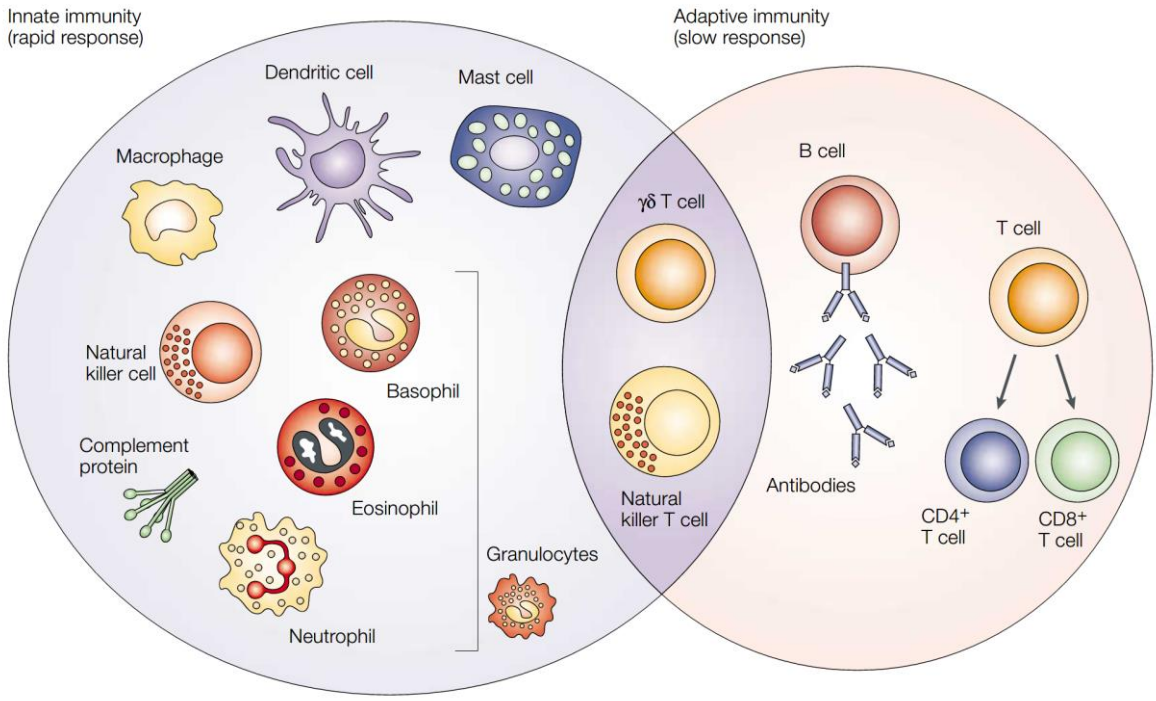

Figure 4: Cells of the immune system. The immune cells and humoral factors can be divided into two groups, the rapidly responding innate system and the slowly responding adaptive system. Some populations of specialized cells show treats of both groups. Picture taken from (Dranoff, 2004).

The first barrier against exogeneous influences is displayed by the skin and other epithelial tissues. Pathogens that cross this first line of defense are handled by specialized immune cells and soluble factors to avoid an acute infection. An overview of the different immune cells is shown in Figure 4.

In general, the immune system can be divided into the innate and the adaptive immune system, differing in their pathogen specificity and activation cascade. Thereby, a strict discrimination of self and non-self is indispensable to allow control of pathogens, whereas immunopathology by overstimulated leukocytes should be avoided (Chaplin, 2010).

1.3.1 Cells of the Innate Immune System

The innate system displays the early defense against invading pathogens. Starting with soluble factors in biological fluids like lysozyme in saliva or complement proteins in the blood, many cell types contribute differently against pathogens. The recognition is performed via conserved patterns shared by many pathogens.

An important function of the innate immune system is the phagocytosis, the engulfment of foreign particles. This in routinely performed by tissue resident macrophages and neutrophil granulocytes in the blood. This mechanism is important for the elimination of bacteria and fungi which are subsequently killed in the phagosome by acidification and lytic enzymes.

Other cells like basophils or mast cells support the local immune reaction by secretion of histamine which induces a vasodilatation and increase of endothelial permeability to simplify the infiltration of other immune cells.

Tissue resident macrophages display a heterogenous group with distinct subpopulations capable of either phagocytosis of opsonized particles, cytokine production or antigen-presentation. Depending on the activating signals, they either gain a pro-inflammatory phenotype, the M1 polarization, with high expression of pro-inflammatory cytokines like interferon γ (IFNγ), interleukin 6 (IL-6) and tumor necrosis factor α (TNFα) and an increased antigen presentation via major histocompatibility complex class II (MHC-II) leading to activation of the adaptive immune system. The regenerative M2 phenotype is mainly induced after tissue damage and is characterized by anti-inflammatory cytokines like interleukin 10 (IL-10), interleukin 4 (IL-4), or interleukin 13 (IL-13).

Beside these two macrophage subpopulations, specialized macrophages in liver and spleen facilitate important functions in early phases of systemic infections. Hepatic Kupffer cells, the largest macrophage population (Dixon et al., 2013), act as a filter system of the blood,

eliminating foreign particles, including gut bacteria, that passed the intestinal wall (Broadley et al., 2016; Zeng et al., 2016).

Splenic macrophages can be divided into red pulp macrophages and those of the marginal zone by their localization around the lymphocyte-dominated white pulp. Red pulp macrophages mainly perform phagocytosis of aged red blood cells (RBC) and platelets whereas $CD169^{+}$ marginal zone macrophages are indispensable for the immune response against many viruses. For this purpose, the expression of ubiquitin specific peptidase 18 (Usp18) allows viral replication within this restricted site, known as enforced viral replication (Friedrich et al., 2020; Honke et al., 2011).

Together with macrophages, dendritic cells (DC) are capable of presenting antigens via MHC-II to adaptive immune cells and thereby act as a connector between the unspecific but early innate system and the late but very specific adaptive immune system. Next to the conventional DC (cDC), plasmocytic DC (pDC) can produce massive amounts of type I interferon (IFN-I), making them responsible for most of the IFN-I found in the serum.

Natural killer (NK) cells are a cell population that is not fitting to the stereotypical classification. On the one hand, they do not recognize one specific antigen, but detect certain molecular patterns or the absence of MHC-I on target cells and are able to kill these cells. On the other hand, they are derived from a lymphoid progenitor cell and MHC-I plays a major role during activation and lytic capability.

1.3.2 Pattern Recognition Receptors

Many pathogens share common patterns, that allow the identification of many different bacteria or viruses with only a small panel of receptors, the pattern recognition receptors (PRR). Some soluble forms are found in the surfactant, whereas most of them are membrane-bound or intracellular.

The most important intracellular PRR for detecting viruses are the two ubiquitously expressed RNA-sensors retinoic acid inducible gene I (RIG-I) and the melanoma differentiation-associated protein 5 (MDA5). Both detect different species of viral RNA, that are produced during viral replication.

Macrophages and DCs additionally express special receptors, the Toll-like receptors (TLR) on their cell surface or in endosomal membranes. The group of TLR consists of 13 different receptors, though not all of them are found in human or murine cells, that recognize pathogen-associated molecular patterns (PAMP). These include e.g. bacterial wall components as well as double-stranded viral RNA.

TLR stimulation leads to an intracellular signaling cascade, finally inducing expression of several cytokines including IFN-I.

1.3.3 Type I Interferon

Type I interferons are a group of similarly acting cytokines that bind to the same cellular receptor, the type I interferon receptor (Ifnar). The signal of the early species interferon β (IFNβ) and interferon α4 (IFNα4) induces an enhancer loop via different interferon regulatory factors (IRF), resulting in the expression of further IFNα subtypes. Binding of any of these subtypes to the Ifnar activates the pathway of Janus kinase (JAK) and finally results in the expression of many interferon-stimulated genes (ISG), establishing the anti-viral state (Stark et al., 1998; van Boxel-Dezaire et al., 2006). For example, the RNase L degrades intracellular RNA, protein kinase R phosphorylates the α-subunit of eukaryotic initiation factor 2 (eIF2α), both leading to decreased expression of viral and cellular genes and can even induce apoptosis of the infected cell.

Furthermore, IFN-I plays a critical role in activation and proliferation of NK cells and cytotoxic T lymphocytes (CTL) (Kolumam et al., 2005; Madera et al., 2016).

1.3.4 Antigen Presentation via Major Histocompatibility Complex

For antigen-specific cell activation antigen presentation is ineligible. To discriminate between antigens that were produced intracellularly and those that were phagocyted, two MHC classes were defined. MHC class I consists of three similar proteins, human leukocyte antigen A (HLA-A), -B and -C in humans and H-2K, H-2D, H-2L in mice, each coupled to a β2-microglobulin. They present peptides from all newly translated proteins, mostly host-proteins but in case of a viral infection or malignancy also foreign antigens.

In contrast to MHC-I, which is expressed in every nucleated cell, MHC class II expression is restricted to antigen-presenting cells, that phagocyte extracellular antigens and present them to T cells via MHC-II. Similarly, the group of MHC-II proteins consists of HLA-DR, HLA-DQ and HLA-DP in humans and H-2 I-A and H-2 I-E in mice.

The MHC genes show high interindividual variability allowing the efficient presentation of many different peptides. But they also play a key role during allograft compatibility, giving the Major Histocompatibility Complex its name (Copelan, 2006).

13.5 Adaptive Immune System

In contrast to the innate immune system, which responds to a variety of pathogens after recognition via a PRR, adaptive responses require previous activation through antigen-presenting cells but are highly specific and effective against the target.

1.3.6 T cells

The specificity of T cells is reached by a broad panel of T cell receptor (TCR) gene fragments for the α and the β chain, that are randomly assembled to a complete gene, giving up to 10^{18} different TCRs in humans (Attaf et al., 2015). This somatic recombination is performed during T cell maturation in the thymus, where self-reactive T cells and those that do not bind to the MHC proteins are negatively selected. Thereby, only very few of the precursors survive and migrate into secondary lymphatic organs to wait for the specific non-self-antigen. The pool of naïve T cells is composed of about 25 million distinct TCRs (Arstila et al., 1999), many of them remaining unused during lifetime.

There are several different subtypes of T cells, differing in required presentation of antigens and induced actions after antigen recognition. The two major groups are the $CD4^+$ helper T cells and the $CD8^+$ cytotoxic T cells.

$CD8^+$ T cells detect MHC-I presented antigens, allowing the recognition of cells that produce non-self-proteins like viral proteins or tumor neoantigens. After antigen recognition, the $CD8^+$ T cell kills the presenting cell either by release of perforins or granzymes, proteins that disrupt the cellular membrane, or induce the endogenous apoptosis pathway by binding to Fas.

In contrast to the cytotoxic T cells, the $CD4^+$ T cells act as conductors of the immune response. They recognize MHC-II presented antigens and give a stimulatory signal to the presenting cell, increasing their ability to act against the phagocyted pathogens. For example, only stimulated macrophages are able to overcome mycobacteria-induced inhibition of the phagolysosome maturation (K. H. Bhat & Yaseen, 2018) and B cells require T cell signals for the antibody class switch.

While most of the $CD4^+$ T cells give an activating signal, a small subpopulation expressing the transcription factor forkhead-box-protein P3 (FoxP3) are suppressive regulatory T cells. Those inhibitory cells are indispensable to limit an immune response and to avoid autoimmunity. Defects in the FoxP3 gene cause the very rare but severe autoimmune syndrome immunodysregulation polyendocrinopathy enteropathy X-linked (IPEX) (Barzaghi et al., 2012).

1.3.7 Antibodies

The second group of adaptive immune cells are the B cells. Their B cell receptor (BCR) genes for heavy and light chain pass a comparable recombination process during the maturation in the bone marrow like the TCR genes do in the thymus. Additionally, the heavy chain ends with one of five constant domains c_μ, c_δ, c_γ, c_ε and c_α. The used domain defines the five classes of immunoglobulins (Ig): IgM, IgD, IgG, IgE and IgA. In brief, IgD is mainly found on the

membrane of early B cells and is secreted in small amounts during viral infection, but the exact role during infection remains unknown (Moskophidis et al., 1997). IgM is a pentamer that is produced early after antigen recognition and is a potent activator of the complement system.

After antigen recognition and receiving an activating signal of a helper T cell, the B cell can switch to IgG, IgE or IgA, antibody classes with higher affinity to the target antigen. These monomeric (IgG, IgE) or dimeric (IgA) immunoglobulins are then produced by terminally differentiated plasma cells and released into the blood or other body fluids. The most prevalent Ig in the plasma is the IgG, whereas IgA is secreted into fluids of the inner surface like saliva, bronchial mucus, tear fluid or intestinal secrets. IgE is important for the defense against parasites but is also responsible for many allergic reactions.

Antibodies (Ab) have many functions during the complex immune response against pathogens. Antibodies bound to viral particles or bacteria activate the complement system to lyse the particle and opsonize for phagocytosis by macrophages via their Fc-receptors.

Besides this mediation between pathogens and other components of the immune system, antibodies are also able to inactivate the virus by binding to the viral entry receptors and thereby blocking the attachment to the host cell. This process is called neutralization, defining neutralizing antibodies (nAb). nAb offer long-term protection against the pathogen by neutralizing the particles before infection of cells occurs. The titer of nAb is often used as surrogate marker for vaccination success against a virus or bacterial toxin, e.g. vaccination against Hepatitis B virus (Hofmann & Kralj, 2009).

1.4 Immune Response against LCMV

LCMV is one of the most used organisms in the field of immunology. Due to this, a lot is known about the different facets of the immune response after systemic infection of mice.

LCMV's natural host is *Mus musculus*, the standard model organism for immunological research, which makes it a favorable tool to study the immune response. Furthermore, many different LCMV strains are available. Some of them induce an acute infection that is controlled within 6 - 20 days, depending on strain and dose, others result in a chronic infection that can be used to study T cell exhaustion and infection-borne immunosuppression (X. Zhou et al., 2012).

To give an overview on expected immune reactions, some of the described phenotypes have been observed using the non-permissive strain Armstrong. At least activated signaling pathways are expected to be similar to the WE strain used in this work.

Infection of mice with the LCMV strain WE results in an acute infection that is controlled in wildtype mice but not in mice deficient for T and B cells (e.g., NOD.SCID).

1.4.1 Innate Response

The early phase of immune response is characterized by high serum levels of pro-inflammatory cytokines and IFN-I.

After systemic application of LCMV, the virus binds its cellular receptor and is internalized by endocytosis. Inside the endosomes, the viral RNA is recognized by endosomal TLR7 and TLR8 at a very early timepoint. Additionally, RIG-I and MDA5 detect intracellular RNA species of replicating viruses, giving increased serum levels of IFNα peaking after 24 hours and decreasing from 72 hours on, exact kinetics differ between used LCMV strains and doses (Norris et al., 2013).

Additionally to the recognition of RNA, TLR2 plays a role in induction of IL-6 and monocyte chemotactic protein 1 (MCP-1) in mice (S. Zhou et al., 2005) and in isolated glial cells (S. Zhou et al., 2008), when infected with LCMV-Armstrong. TLR2 is a PRR that normally detects lipoteichoic acid (LTA) of gram$^+$ bacteria, but also glycoprotein B of Herpes simplex virus (HSV-1) (Cai et al., 2013) and other viruses (Barbalat et al., 2009) and finally stimulates the cytokine production via nuclear factor kappa-light-chain-enhancer of activated B cells (NF-κB).

1.4.2 Adaptive Response

Like in many viral infections, activation of the adaptive immunity is ineligible for the clearance of LCMV.

Low to medium doses of acute LCMV strains like WE or Armstrong induce strong CD8$^+$ T cell responses. At day 8, up to 90 % of circulating CD8$^+$ T cells show an effector phenotype and so seem to be virus-specific (Masopust et al., 2007). These activated T cells are sufficient for virus elimination even in the absence of antibodies (Straub et al., 2013), but may also cause immunopathology in infected organs. LCMV-WE can be used as a model for virus-induced hepatitis with a temporary increase in transaminase levels (Zinkernagel et al., 1986).

When LCMV, especially neurotropic strains like Armstrong, pass the blood-brain-barrier or are injected intracranially, the resulting infiltration of T lymphocytes leads to a choriomeningitis, giving the virus its name, which can be fatal in certain doses. In the absence of virus-specific T cells e.g., in knock-out mice or those with a transgenic and irrelevant TCR, virus replication occurs in the central nervous system (CNS) without any symptoms. Transfer of virus-specific T cells reconstitutes this pathology (McGavern & Truong, 2004), underlining the importance of viral clearance before the virus can pass the blood-brain-barrier.

While the development of anti-viral T cells is supported by IFN-I (Kolumam et al., 2005), early IFN-I signaling on B cells reduces their ability to produce specific antibodies and increases hypergammaglobulinemia (Daugan et al., 2016).

In general, many viral infections are terminated by neutralizing antibodies, that prevent the infection of cells and allow complete clearance of the virus. In case of LCMV, six N-linked glycosylation motifs in the GP1 ("glycan shields") prevent antibodies from binding to the receptor recognizing epitope (Sommerstein et al., 2015). Therefore, it is quite rare that neutralizing antibodies develop in C57BL/6 mice. Only decreased function of $CD8^+$ T cells and resulting viral persistence for more than 30 days in combination with intact function of B cells and $CD4^+$ T cells enables the required somatic hypermutation of B cells. This occurs e.g. in *Cd8a*$^{-/-}$ or CD8-depleted mice (Recher et al., 2004).

Despite this, non-neutralizing antibodies are useful to control infections with high doses and may prevent chronic infections (Richter & Oxenius, 2013).

1.5 *In Vivo* Tumor Models

To investigate the effect of anti-tumoral therapies in a mouse model, a standardized and reproducible way to engraft tumors in mice is indispensable. The subcutaneous injection of tumor cells leads to formation of a tumor, that is easy to access and to measure during growth. This allows a frequent observation of tumor growth without harming the mouse during the experiment.

Depending on the origin of the tumor cells, murine (syngeneic) or human (xenograft) tumors can be engrafted, enabling the investigation of murine and human tumor models.

1.5.1 Syngeneic Models

Tumor cells that derive from inbred mouse strains like C57BL/6 or Balb/c can be engrafted in the corresponding mice due to the same genetic background (syngeneic).

This offers a model with immunocompetent mice, displaying all anti-tumor mechanisms that humans have in a clinical setting, with the possibility to investigate all effector arms, including T cell responses, without the risk of tumor rejection due to MHC incompatibility.

On the other hand, many of these murine tumor cell lines are chemically induced or immortalized by genetic engineering and behave different to corresponding entities in humans.

Nevertheless, models can be divided into different groups, that differ in certain histological patterns like mutational burden or immune infiltration that gives rise to the classification as "hot" or "cold" tumors (Mosely et al., 2017).

Hot tumors are characterized by many mutations resulting in many neoantigens that can be detected by infiltrating T cells. Exhaustion of T cells with upregulation of inhibitory receptors like programmed cell death protein 1 (PD-1) are the common issues with those tumors making them a favorable target for checkpoint inhibitor e.g., anti-PD-1 antibodies (Liu & Sun, 2021).

In contrast, cold tumors show only few immune cells, often exhibiting an inhibitory phenotype. Due to the lack of neoantigens and T cells, cold tumors are usually resistant to checkpoint blockade (Liu & Sun, 2021).

1.5.2 Xenograft Models

Subcutaneous implantation of human tumor cells gives the opportunity to examine the effect of therapeutic approaches in human models, that were initially isolated from human patients. This allows the assumption of direct knowledge transfer to real clinical cases.

Unfortunately, human cells are rejected in immunocompetent mice due to the MHC incompatibility. Therefore, it is inevitable to use immunocompromised mice, deficient in T and B cells e.g., NOD.SCID mice. These mice are homozygote for a spontaneous mutation in the protein kinase, DNA-activated, catalytic subunit (*Prkdc*) gene giving the “scid”-allele, short for severe combined immunodeficiency. The introduced early stop-codon functionally knocks out the gene. Due to the lack of the *Prkdc*, a protein kinase involved in the somatic recombination of T and B lymphocytes, their precursors are unable to differentiate and finally, mice do not reject xenograft tumors, but also do not show any anti-tumoral or anti-viral T cell response.

1.6 Current Virotherapeutical Approaches

For many patients, the classical therapies including surgery, chemotherapy and irradiation show only limited success in later stages and are often associated with severe side effects. The upcoming use of targeted therapies in the last two decades significantly improved the outcome, while checkpoint inhibitors like PD-1 or cytotoxic T lymphocyte antigen 4 (CTLA-4) blocking antibodies give a hint which overwhelming potential the immune stimulatory therapies might have (Robert, 2020).

To make use of the immune stimulatory potential, many different approaches use live-attenuated or replication-deficient viruses to induce an anti-tumoral effect without severe side effects. Viral approaches can be divided into two different classes: oncolytic viruses and virus-based tumor vaccines.

Oncolytic viruses are replication-competent viruses that exclusively replicate in tumor cells and lyze them through their cytolytic capacity. Talimogene laherparepvec (Imlygic®) from Amgen is the first virus approved for late-stage malignant melanoma therapy in Germany (Andtbacka et

al., 2015). To increase the tumor tropism of the HSV-1, genes for infected cell protein 34.5 (ICP34.5) and infected cell protein 47 (ICP47), two viral immune escape mechanisms, were deleted and the human colony-stimulating factor 2 (*CSF2*) gene, encoding for the chemotactic granulocyte-monocyte colony-stimulating factor (GM-CSF), was inserted to increase the immune infiltration into the tumor tissue.

Another promising candidate is the VSV-GP from ViraTherapeutics. It is based on the Vesicular stomatitis virus (VSV), a fast replicating and cytopathic virus, able to lyse infected tumor cells. Unfortunately, the wildtype VSV glycoprotein (VSV-G) shows a strong neurotropism leading to paralysis and consecutive death of infected mice. To overcome this, the gene for VSV-G was replaced by the gene for the LCMV-GP, giving this hybrid virus the natural tropism of LCMV-WE (Muik et al., 2014).

In contrast to oncolytic viruses, virus-based vaccines are not supposed to lyse the tumor cell directly but stimulate the immune system against vaccinated tumor antigens. A prominent example for this mode of action is Hookipa using the non-cytopathic LCMV with a GP-gene replaced by a selectable antigen, thereby abrogating the ability to replicate but vaccinating against the antigen (Flatz et al., 2010; Schwendinger et al., 2020).

Another approach is the use of tri-segmented LCMV, bearing one L- and two S-segments (see 1.1.1 Viral Structure). In each of the S-segments, one of the two open reading frames (ORFs) is replaced by a tumor antigen. This allows the insertion of two different antigens and preserves the replication capacity of the virus (Kallert et al., 2017).

The idea of this work is based on previous work of Kalkavan et al. showing the general efficacy of wildtype LCMV as immune-stimulatory virus to induce tumor regression (Kalkavan et al., 2017). Starting from this finding, the used LCMV strain WE was optimized by the Fast Evolution Platform (see 1.2.1 Fast Evolution Platform) to obtain a mutant virus having improved anti-tumoral properties in syngeneic and xenograft models.

1.7 Aim of this Work

Viral therapies represent a promising new approach in cancer treatment. Kalkavan et al. already proved the general capability of LCMV-WE to induce an anti-tumoral immune response. In order to even improve these properties and to reduce systemic side effects of the viral therapy, a change of tropism towards malignant cells was supposed to be beneficial.

For this purpose, this works includes the following working steps:

1) The wildtype LCMV strain WE is passaged several times on human Non-Small Cell Lung Cancer (NSCLC) cell line H1975 to obtain a virus with tropism for tumor cells.
2) The stability of the passaged virus is tested by further passages on the same cell line.
3) This mutant virus is characterized *in vitro* for its replication in tumor cells.
4) The mutant virus is characterized for its capacity to activate the innate and adaptive immune system *in vivo*.
5) The mutant virus is compared to the wildtype strain in concerns of its anti-tumoral effect in a human tumor model.
6) If more than one mutation occurs, discrimination of different mutations is desired if possible.

2. Materials and Methods

2.1 Materials

2.1.1 Media / Buffers

Table 1: Materials used for cell culture

Medium / Buffer	Company
Dulbecco's Modified Eagle's Medium (DMEM)	PAN Biotech
Fetal Calf Serum (FCS), heat-inactivated	Gibco
Penicillin-Streptomycin-Glutamine (100X)	Gibco
Phosphate Buffered Saline (PBS)	PAN Biotech
Roswell Park Memorial Institute Medium (RPMI-1640)	Biochrom
Trypsin 0.25 % / EDTA 0.02 % in PBS	PAN Biotech
Very Low Endotoxin (VLE) DMEM	Biochrom
β-Mercaptoethanol (β-ME)	Sigma-Aldrich

Table 2: Self-made buffers

Buffer	Components
Blocking Buffer	PBS + 10 % FCS
BMDM Lysis Buffer	155 mM NH_4Cl + 10 mM $KHCO_3$ + 150 µM EDTA, pH 7.8
BMDM medium	VLE DMEM + 10 % FCS + 0.1 % β-ME + 10 % L929-conditioned medium (sterile-filtered)
FACS Buffer	PBS + 2 % FCS + 2.5 mM EDTA
FACS Perm Buffer	PBS + 2 % FCS + 2.5 mM EDTA + 0.2 % (w/v) Saponin
Histology Staining Buffer	PBS + 2 % FCS

2.1.2 Reagents

Table 3: Reagents for cell and mouse work

Reagent	Company
Brefeldin A	Sigma-Aldrich
Citric acid	Sigma-Aldrich
Dimethyl sulfoxide (DMSO)	Sigma-Aldrich
FACS Counting Beads	BD Bioscience
FACS Lysing Solution	BD Bioscience
Fluorescent Mounting Medium	Dako
Formalin	AppliChem
Gel Loading Dye, Purple (6X)	New England Biolabs
H_2O_2	Sigma-Aldrich
IFN alpha Mouse ELISA Kit	ThermoFisher
Isoflurane	Piramal CriticalCare
Na_2HPO_4	Sigma-Aldrich
o-Phenylendiamine	Sigma-Aldrich
Pam_2CSK_4	Sigma-Aldrich
Peptides	Anaspec
Tetramer, H-2D^b, loaded with GP33	NIH, Tetramer Facility
TissueTek O.C.T. medium	Takara
Triton X-100	Sigma-Aldrich

Table 4: Reagents for RNA and sequencing

Reagent	Company
Chloroform	Merck
Nuclease-free Water	Ambion
Dithiothreitol (DTT)	Invitrogen
dNTPs, 10 mM each	New England Biolabs
Ethanol	Honeywell
Ethidium bromide	Carl Roth
iProof High-Fidelity DNA Polymerase	Bio-Rad
Isopropanol	Merck
Mag-Bind TotalPure NGS	Omega Bio-Tek

Primer	Eurofins Genomics
Q Solution	Qiagen
QIAamp Viral Mini Kit	Qiagen
QuantiTect Reverse Transcription Kit	Qiagen
RNase H	New England Biolabs
RNase Inhibitor (murine)	New England Biolabs
SuperScript IV Reverse Transcriptase	Invitrogen
SYBR Green Fast Mastermix	Applied Biosystems
TRIzol	Ambion

Table 5: Antibodies

Antibody	Clone	Label	Company
α-LCMV-NP	VL4	none	Self-made from Hybridoma
α-CD169	3D6.112	FITC	amsbio
α-CD8	53-6.7	PE-Cy7	eBioscience
α-IFNγ	XMG1.2	APC	eBioscience
α-TNFα	MP6-XT22	eFluor 450	eBioscience
α-PD-1	RMP1-14	none	BioXcell
α-rat-IgG	polyclonal	PE	Jackson Immunoresearch

Table 6: cell lines

Cell line	species	tissue	Provided by
MC57G	Mouse	Fibrosarcoma	ATCC
BHK-21	Hamster	Kidney	ATCC
H1975	Human	NSCLC	ATCC
SW872	Human	Liposarcoma	ATCC
HCC1954	Human	Breast carcinoma	ATCC
B16-Ova	mouse	Melanoma, expressing Ovalbumin	Percy Knolle, TU München

Table 7: single-use materials

Material	Company
Syringe, 29G	Becton Dickinson
Micro-hematocrit capillaries	Hirschmann
Metal ball	Qiagen
1.5 mL tube	Eppendorf
2 mL tube	Eppendorf
15 mL conical tube	Greiner Bio-One
50 mL conical tube	Greiner Bio-One
1.8 mL cryotube	ThermoFisher
Histology tube	Carl Roth
Cell strainer, 70 µm	Corning
Cell scraper	Corning
Cell culture flask, T25 / T75 / T175	ThermoFisher
Cell culture plate, 24-well / 96-well / 12-well	TPP
qPCR plate, 384-well, white	Roche
Microscopy slides	Marienfeld
Cover slips	Marienfeld

Table 8: Primers

Name	Sequence	Use
LCMV 3'	*CGCACAGTGGATCCTAGGC*	Reverse Transcription
PS1f	*GGATCCTAGGCTTTTTGGATTGCGC*	PCR S segment part 1
PS1r	*AACCGTTCACAACATCCTGCCACATG*	PCR S segment part 1
PS2f	*CAAGGTGCCTGGTGTAAAAACTATCTGG*	PCR S segment part 2
PS2r	*GTGGATCCTAGGCATTTGATTGCGC*	PCR S segment part 2
PL1f	*GGGATCCTAGGCGTTTAGTTGCGC*	PCR L segment part 1
PL1r	*AGGCTCACCGTGACCACATCAACC*	PCR L segment part 1
PL2f	*GCCTAACAGCCGAATTACTCTCGTTC*	PCR L segment part 2
PL2r	*CAAAGGAGACCCCTGATAGATTGACAGATC*	PCR L segment part 2
PL3f	*CCAAACTCACTCTTGGGCTCAAAGAAC*	PCR L segment part 3
PL3r	*CTAGGCTTTTTGATGCGCAATGGATG*	PCR L segment part 3
SeqS1.1	*CAAAGGCAGTTCTAAACATGTCCAAGACTC*	Sanger seq of PCR S1
SeqS1.2	*CACCAGTCTTAGCATGTTCCAGATACC*	Sanger seq of PCR S1

SeqS1.3	*CAAGATGTAGAGTCTGCCTTGCATG*	Sanger seq of PCR S1
SeqS2.1	*TGTTGAAAGACTTGATGGGAGGGATTGATC*	Sanger seq of PCR S2
SeqS2.2	*GCCCATTTTGTGGTTGGAATATTGCTATC*	Sanger seq of PCR S2
SeqS2.3	*GTCTGTGACTGTTTTGCCATGCAAGC*	Sanger seq of PCR S2
SeqL1.1	*GCGCTGCTTTATTGCACAGCTTC*	Sanger seq of PCR L1
SeqL1.2	*ATTACAGTGTTCTTTGACCTGCTGAAGC*	Sanger seq of PCR L1
SeqL1.3	*AATTAACATAGCGGCATTACACACAACATC*	Sanger seq of PCR L1
SeqL1.4	*GATTCAGAACTGGTGAGCACTTGATGG*	Sanger seq of PCR L1
SeqL2.1	*GTTAAACACTCACACTGATGTAAAGGATTGG*	Sanger seq of PCR L2
SeqL2.2	*GTGATGTAGTCTTCTTACAAGTTTTCTCATGATC*	Sanger seq of PCR L2
SeqL2.3	*CAGGTAAAAGAGCTTATCTGAGGAAAGTC*	Sanger seq of PCR L2
SeqL2.4	*CAGCCTCACAAATAAACCTCATGTCGTC*	Sanger seq of PCR L2
SeqL3.1	*CATTTGCTGAATTTGAGAACTTTATGAGAGC*	Sanger seq of PCR L3
SeqL3.2	*CTCAAACTCTGTAAACCCCTCAATTGCTC*	Sanger seq of PCR L3
SeqL3.3	*CCTTTTGAGTTTCCCATTTAACAGGTCCCTC*	Sanger seq of PCR L3
Gapdh	Qiagen QT01658692	qPCR
Ifnb1	Qiagen QT00249662	qPCR
Tnf	Qiagen QT00104006	qPCR
Ccl2	Qiagen QT00167832	qPCR
Ccl5	Qiagen QT01747165	qPCR
Il1b	Qiagen QT01048355	qPCR
Il6	Qiagen QT00098875	qPCR
Nos2	Qiagen QT00100275	qPCR

2.2 Methods

If not mentioned differently, all solutions are considered aqueous, and all steps were performed at room temperature (20 – 25 °C).

To ensure sterility and personal safety, all work with live organisms, including cells, mice, and viruses, were performed under a class II biosafety cabinet (BSC).

Standard conditions for incubating cells were 37 °C with 5 % CO_2 atmosphere in a humidified incubator.

2.2.1 Cells

2.2.1.1 Cell culture

To obtain complete growth medium (CGM) DMEM was supplemented with 10 % FCS for H1975 and SW872 cells or 5 % FCS for MC57G and BHK-21 cells. For HCC1954, RPMI-1640 supplemented with 10 % FCS was used as CGM. All media were additionally supplemented with 100 U/mL penicillin, 100 µg/mL streptomycin and 292 µg/mL L-glutamine.

To subculture adherent cells, growth medium was removed, and cells were washed once with PBS. Trypsin/EDTA was added and incubated for 3 - 5 min at 37 °C. Flasks were gently tapped to detach cells completely and the protease activity was stopped by addition of 10 mL CGM, followed by reseeding of desired volume of cell suspension.

If the cells were used for an experiment, the cell suspension was centrifuged for 5 min at 400 x g at 4 °C. After aspiration of supernatant, cells were resuspended in fresh CGM and counted with a Neubauer counting chamber.

2.2.1.2 Freezing and Thawing of Cells

Due to the genomic instability of tumor cells, longer passaging of cells reduces the reliability of experimental results. To overcome this problem, cells were frozen down at early passages and thawed from time to time, to have only cells with low passage number in use.

To freeze cells, DMSO was added to the cell suspension to a final concentration of 7.5 %. This suspension was immediately transferred into a cryovial and placed in an isopropanol containing box. This allows a slow freezing process when placed in a -80 °C freezer, with a rate of 1 K/min. Frozen cells were either stored at –80 °C or in liquid nitrogen for long-term storage.

To restart the cell culture from frozen cells, the cryovial was placed in a 37 °C water bath until there was only a small ice crystal left and directly transferred into a culture flask with prewarmed CGM. After 4 h, when the viable cells became adherent, the supernatant was removed and replaced with fresh CGM. When the cells recovered their morphology and growth rate, they were used for experiments.

2.2.1.3 Stimulation of TLR2

To stimulate bone marrow-derived macrophages (BMDM, see 2.2.6.8 Bone Marrow-Derived Macrophages for generation) *in vitro*, 5 x 10^5 differentiated BMDM were plated with BMDM medium in a 12-well plate and incubated overnight to allow adherence. Stimulation with virus stocks was performed by adding 1 µL of serum-free virus stocks, adjusted to 1.5 x 10^9 FFU/mL, giving a multiplicity of infection (MOI) of 3 with the lowest possible volume to reduce effects of the suspension medium to adherent macrophages. The virus stocks were produced in-house

and kindly provided by Sarah-Kim Friedrich-Becker. The control cells were treated with cell supernatant of uninfected producer cells. As positive control, Pam_2CSK_4, a synthetic TLR2/6 agonist was used in a final concentration of 100 ng/mL, diluted in PBS.

After 2 h incubation at 37 °C, medium was removed, and cells were washed once with PBS. Cells were harvested with 1 mL TRIzol and immediately snap-frozen in liquid nitrogen.

2.2.3 Viruses

2.2.3.1 Virus Passage

Virus passage was performed by repeated infection of human lung carcinoma cells H1975. Therefore, 2 x 10^5 cells were seeded in 1 mL CGM into a well of a 24-well plate and infected with virus. For the first passage cells were infected with LCMV strain WE with an MOI of 1.

After 72 h, 10 µL of the virus containing supernatant were transferred to the next well with again 2 x 10^5 naïve H1975 cells. The remaining supernatant was stored at -80 °C for later analysis. These steps were repeated for each passage.

2.2.3.2 Virus Stock Generation

For a virus mutant, a working virus stock was produced under controlled conditions.

For virus stock production, BHK-21 cells were cultured in a T175 flask to 60 - 70 % confluence in CGM. For initial infection, medium was removed from adherent cells and replaced by 5 mL DMEM + 2 % FCS, containing 2 x 10^4 FFU of desired virus. After 20 min incubation at 37 °C, additional 25 mL DMEM + 2 % FCS were added, and cells were incubated for 48 h in the incubator.

Thereafter, supernatant was transferred into a 50 mL tube and centrifuged for 20 min at 3,220 x g at 4 °C to remove cell debris. The clarified supernatant was then aliquoted and stored at -80 °C. Before the stock was used, virus titer was determined by focus-forming assay (see 2.2.3.3 Focus-forming Assay) and diluted to desired concentrations and verified by focus-forming assay. This allowed the use of equal volume for all viruses even with different titers of original stocks.

2.2.3.3 Focus-forming Assay

To quantify the number of infectious particles per mL, samples were titrated, and dilutions were transferred onto MC57G cells and overlayed with methylcellulose. Two days later, infected foci were visualized by immunocytochemistry.

In detail, a suspension of MC57G cells was prepared to a final density of 5 x 10^5 cells/mL.

96-well plates were prepared by adding 135 µL DMEM + 2 % FCS in row 2 - 12 (see Figure 5: Titration Scheme, grey). 200 µL of sample were added to row 1 in duplicates and diluted from row 1 to 12 by transferring each 65 µL. This results in a 1:10 dilution every second row.

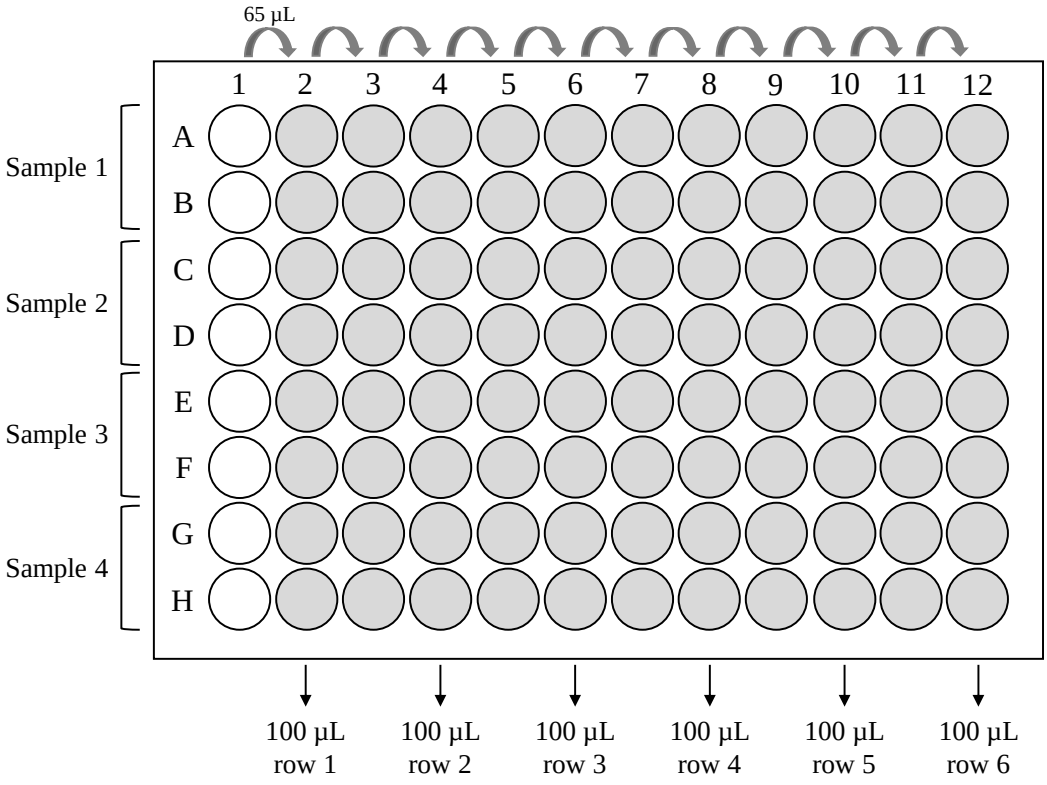

Figure 5: Titration Scheme.

Finally, 200 µL of the cell suspension were transferred to each well of a 24-well plate and sample dilutions were added as indicated in Figure 5.

Four hours later, when the cells attached to the plate and all infectious viruses bound to a cell, the cells were overlayed with methylcellulose to avoid release of new viral particles and to allow focus formation.

After two days, the cells formed a confluent monolayer and each infectious virus induced one focus, which was then visualized by immunocytochemistry staining.

Therefore, the infectious supernatant was removed under a biosafety cabinet and the cell layer was fixed with 4 % Formalin in PBS for 30 min. After fixation, the cells were permeabilized by 20 min incubation with 1 % Triton X-100 in PBS, followed by two washing steps with PBS. To block unspecific binding of antibodies, samples were incubated with PBS containing 10 % FCS for one hour. The cells were then incubated with a rat-IgG against the viral nucleoprotein (clone VL4) and a polyclonal antibody against rat-IgG conjugated to horseradish peroxidase (HRP).

Between each step, the plates were washed twice with PBS. Finally, an aqueous solution with 50 mM Na_2HPO_4, 25 mM citric acid, 0.045 % H_2O_2 and 1 tablet (20 mg) of o-phenylenediamine (OPD) per 50 ml was added. The antibody conjugated HRP oxidized the OPD to 2,3-diaminophenazine, an insoluble brown product, making the foci visible. After washing and drying, the foci were counted at a dilution with 10 to 100 foci per well, and the viral titer was calculated via Equation 1.

Equation 1: calculation of viral titer

$$viral\ titer\ [FFU/mL] = counted\ foci * 15 * 10^{well-1}$$

2.2.3.4 Neutralization Assay

To evaluate the neutralizing capacity of sera, serial dilutions of sera were UV-inactivated, incubated with virus stock and remaining infectious titer determined.

For dilutions of sera, 5 µL of serum was added to 45 µL DMEM +2 % FCS in column 1 of a 96-well flat bottom plate, giving an initial dilution factor of 10. Before, 25 µL of dilution medium was prepared in columns 2 - 12, allowing serial dilutions of sera each with 1:2 per column.

To inactivate viral particles in the serum, dilution plates were UV-inactivated (see 2.2.3.7 UV-Inactivation). Afterwards, 20 FFU LCMV were added in 25 µL to each well and plates were incubated for 1.5 h at 37 °C.

Finally, 3 x 10^4 MC57G cells were added in 50 µL DMEM +5 % FCS, overlayed with methylcellulose after additional 4 hours and stained after two days as described in 2.2.3.3 Focus-forming Assay.

2.2.3.5 Subcloning of Virus

To obtain single mutant viruses, subcloning of mixed stocks and passages was performed. 5 x 10^4 BHK-21 cells were seeded in a 24-well plate and infected with different titrations of the virus stock per row.

Starting with the titer measured by focus-forming assay, virus-containing sample was diluted with DMEM + 2 % FCS to a final concentration of 50 FFU/mL. This material was used as starting point for 3 dilution steps as described in 2.2.3.3 Focus-forming Assay. 200 µL of respective dilution was added to the cells in six replicates. Statistically, the lowest row contained < 1 FFU per well.

After 72 h, supernatant was sampled and stored, and the cells were stained as described in 2.2.3.3 Focus-forming Assay. The brown staining reveals the initial presence of at least one virus

particle. If the staining was only detectable in a few wells of the same dilution, the limiting dilution was successful.

The stored supernatant of 3 - 5 clones was used for sequencing (see 2.2.4 Virus Sequencing) and clones with the desired sequence were used to produce new stocks as described in 2.2.3.2 Virus Stock Generation.

2.2.3.7 UV-Inactivation

To inactivate LCMV particles without disrupting proteins, ultraviolet (UV) light can induce dimers in DNA and RNA and thereby inhibits the transcription of the viral genome.

For inactivation, the UV light source of the BSC was used. To gain maximum efficiency, the distance to the light source was minimized as possible, and liquids were placed in plates or dishes without lid, allowing maximum surface for 2 x 10 min, with shaking in between. In earlier tests, efficacy of virus inactivation was proved by focus-forming assay and RT-qPCR.

2.2.4 Virus Sequencing

For the characterization of the passaged virus and working stocks and the identification of mutations compared to the wildtype LCMV strain WE, sequencing of the viral genome was performed. Therefore, viral RNA was isolated from supernatant, transcribed to complementary DNA, amplified by polymerase chain reaction (PCR), and finally sent to Microsynth Seqlab for sequencing.

2.2.4.1 RNA Isolation

For RNA isolation, the QIAamp Viral RNA Mini Kit from Qiagen was used according to manufacturer's instructions. In brief, supernatant was mixed with lysis buffer and ethanol and mixture was transferred to a silica membrane that specifically binds RNA. After two washing steps RNA was eluted in nuclease-free water and used for reverse transcription.

2.2.4.2 Reverse Transcription

The cDNA synthesis was performed with the SuperScript IV RT according to manufacturer's protocol.

In brief, the RNA was mixed with dNTPs and the genome-specific primer (LCMV 3') and placed for 5 min at 65 °C, in order to denature the RNA and anneal the primers. After direct cooling on ice, SuperScript RT buffer, DTT, RNase inhibitor murine and the SuperScript IV RT were added. The samples were incubated in a thermocycler for 15 min at 55 °C and 10 min at 80 °C. After cooling to 37 °C, RNase H was added and incubated for 20 min at 37 °C to remove genomic RNA after successful cDNA synthesis.

2.2.4.3 PCR of Genomic Subsegments

To obtain sufficient amount of template for the desired Sanger sequencing, single-stranded cDNA was amplified with five PCRs, producing the segments S1, S2, L1, L2 and L3 as shown in Figure 6.

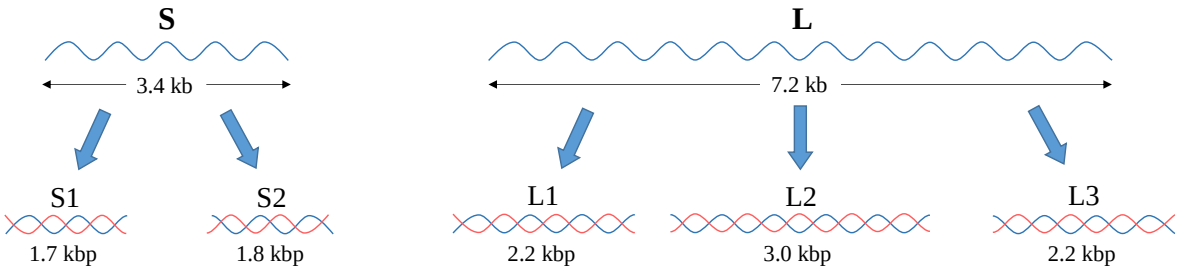

Figure 6: PCR of genomic subsegments. The single-stranded cDNA of the genomic S and L segment is amplified in two or three subsegment between 1.7 and 3.0 kilobase pairs (kbp).

For the PCR setup, 25 µL nuclease-free water, 10 µL 5X iProof HF buffer, 1 µL dNTPs, 10 µL Q solution, 0.5 µL iProof High-Fidelity DNA Polymerase and 2.5 µL of the respective primer pair (10 µM each, see Table 8: Primers) were mixed and 1 µL cDNA template was added. The following settings were used for the thermocycler.

Table 9: PCR Settings

	Initial Denaturation:	03:00	at 98 °C
35 cycles	Denaturation:	00:15	at 98 °C
	Annealing:	00:30	at 63 °C
	Elongation:	02:00	at 72 °C
	Final Elongation:	10:00	at 72° C

2.2.4.4 Gel Electrophoresis and PCR Purification

To verify the correct length of the amplicons, 5 µL of the PCR product were mixed with 1 µL 6X DNA loading dye and together with the NEB 1kb plus ladder loaded onto a 1.5 % agarose gel with 0.1 µg/mL ethidium bromide. The voltage was set to 120 V and after 45 - 60 min, DNA bands were visualized by UV excitation. If bands of the desired size were visible, the PCR product was purified with magnetic beads. In brief, magnetic beads were mixed with the PCR product and placed on a magnetic separator, which was self-designed and 3D-printed. After two washing steps with ethanol, DNA was finally eluted with nuclease-free water.

2.2.4.5 Sanger Sequencing and Analysis

Purified PCR products and primers were sent for Sanger sequencing to Microsynth Seqlab.

The results were analyzed with Geneious Prime software by assembly to a whole-genome reference sequence.

2.2.5 RT-qPCR

To gain quantitative expression data of cellular or viral genes, RNA was isolated using TRIzol, reverse transcribed and quantified via a SYBR® Green-based qPCR.

2.2.5.1 RNA Isolation Using TRIzol

Samples of cells were lysed with 1 mL TRIzol. After addition of 200 µL chloroform and vigorous shaking, samples were first incubated for 5 min at room temperature, then centrifuged for 20 min at 21,000 x g at 4 °C.

500 µL of the upper and clear aqueous phase containing the RNA was transferred into a clean 1.5 mL tube. An equal volume of 2-propanol was added, gently mixed by inverting and placed for 15 min on ice, to precipitate the RNA.

After centrifugation at 21,000 x g for 15 min at 4 °C, a small pellet was visible, consisting of RNA and contaminants. To purify the product, supernatant was aspired, and the pelleted RNA was washed twice with 70 % ethanol. Each washing step included a centrifugation for 5 min at 21,000 x g at 4 °C.

Finally, supernatant was removed with a vacuum pump to ensure complete removal of ethanol before RNA pellet was dissolved in an appropriate volume of nuclease-free water and used directly or stored at –20 °C.

2.2.5.2 Quantitative Reverse Transcription

Isolated RNA was quantitatively reverse transcribed using the Qiagen QuantiTect Reverse Transcription Kit according to manufacturer's instructions. In brief, RNA was diluted with nuclease-free water to final amount of 500 ng in 6 µL. Genomic DNA was degraded with the provided gDNA wipeout buffer for 3 min at 42 °C. After addition of 5X RT buffer, random hexamer primers and reverse transcriptase, samples were incubated for 30 min at 42 °C. To inactivate the enzyme afterwards, samples were heated to 95 °C for 3 min. 40 µL nuclease-free water was added to a final volume of 50 µL.

2.2.5.3 Quantitative Polymerase Chain Reaction (qPCR)

Quantitative PCR of cDNA was performed using Fast SYBR® Green Master Mix with Qiagen QuantiTect Primer Assay primers in a Roche LightCycler 480.

5 µL of Master Mix were mixed with 1.5 µL of nuclease-free water, 1.5 µL of respective primer and finally 2 µL of cDNA were added per well in a 384-well plate.

Gapdh was used as house-keeping gene and all CT values were normalized to *Gapdh* of respective sample. Additionally, all normalized values were compared to the mean of naïve cells, giving ΔΔCT. Relative expression was calculated using Equation 2.

Equation 2

$$relative\ expression = 2^{-([CT(gene)-CT(Gapdh)]-[CT(gene\_naive)-CT(Gapdh\_naive)])}$$

2.2.6 Mice

All animal experiments were performed according to the German laws for animal protection and were authorized by the *Landesamt für Natur-, Umwelt- und Verbraucherschutz (Lanuv) Nordrhein-Westfalen*.

All mice were housed in individually ventilated cages, checked daily, and sacrificed with corresponding termination criteria or due to experiment settings. Termination criteria were body weight, general condition, spontaneous behavior, clinical findings, and tumor size.

2.2.6.1 Used Mouse Strains

C57BL/6 mice are a wildtype inbred strain commonly used for immunological studies. To grow human tumors in mice, T and B cell deficient NOD.SCID mice were used for xenograft models. For all experiments 6 - 8 weeks old female mice of required genotype were used. Systemic infection with the used dose of LCMV-WE usually results in only low burden of mice with no visible changes in habitus and only slight temporary weight loss.

2.2.6.2 Infection of Mice

In all experiments, infection of mice was performed by intravenous injection of 2 x 10^4 FFU in 200 µL DMEM + 2 % FCS.

For intravenous injection, the mouse was placed in a restrainer and the lateral tail vein was punctured with a 29G syringe. After slow injection of the prewarmed liquid, the mouse was immediately released and put back into the cage.

2.2.6.3 Subcutaneous Tumor Engraftment

The growth of subcutaneous tumors was induced by injection of tumor cells into the left flank. The cells were previously cultured *in vitro*, detached from the flask, and counted as described in 2.2.1.1 Cell culture. Until injection, the cells were stored on ice to ensure high viability of injected cells.

For subcutaneous injection, the mouse was short-term anesthetized with isoflurane and 1 x 10^6 tumor cells were injected in a volume of 100 µL DMEM into the left flank. After 7 - 10 days, the tumor became palpable, and the mice were treated as indicated.

2.2.6.4 PD-1 Blockade

To block the interaction between PD-1 and its ligand programmed cell death ligand 1 (PD-L1) *in vivo*, mice were treated with 200 µg of an α-PD-1-antibody (clone RMP1-14) given intraperitoneally on day 1, 5 and 8.

2.2.6.5 Bleeding of Mice

To obtain blood samples from mice, the retro-orbital bleeding method was used. For this, the mouse was short-term anesthetized with isoflurane and held by the back of the neck, while tightening the skin to accumulate the blood flow. A heparinized capillary is placed at the medial canthus of the eye and slowly moved forward by simultaneous rotation to slightly injure the retro-orbital venous plexus, without affection the bulbus. The capillary is filled by capillary action and the blood drops are captured in a prepared tube containing either EDTA or gel, depending on further use of the blood samples.

2.2.6.6 Tumor Measurement

The subcutaneous tumors were measured three times per week with a Castroviejo caliper. The estimated volume was calculated according to Equation 3.

Equation 3: Tumor Volume Calculation

$$volume\ [mm^3] = length\ [mm] * (width[mm])^2 * 0.5$$

2.2.6.7 Sacrifice and Section of Mice

When termination criterium was met or the mouse should be sacrificed, the mouse was killed by cervical dislocation.

To remove the organs for further analysis, the mouse was laid on the back and the skin was disinfected with 70 % ethanol. After incision of the skin, subcutaneous organs like inguinal lymph node or tumor were removed. Subsequently, the peritoneum was incised, and the intraperitoneal organs were removed, followed by the retroperitoneal kidney. The lung was accessed via the diaphragm. The last organ routinely removed was the brain. For this purpose, the mouse laid on its stomach, and the neck's skin incised from ear to ear and an additional cut towards the nose. The uncovered skull was punctured with sharp scissors and the brain, was entirely removed, including cerebrum, cerebellum, and brain stem.

During the organ preparation all fat and connective tissue was removed and organs were placed in a 2 mL tube prepared with a metal ball and 1 mL of DMEM with 2 % FCS for focus-forming assay. For histological analysis, organs were placed in cryotubes and surrounded with Tissue Tek. All samples were snap-frozen in liquid nitrogen and stored at -80 °C for later analysis.

Organ sample used for focus-forming assay were thawed and smashed in the Qiagen TissueLyzer II for 10 min at 25 Hz. Afterwards, they centrifuged at 12,000 x g for 5 min to pellet cell debris, and titer was determined as described in 2.2.3.3 Focus-forming Assay.

2.2.6.8 Bone Marrow-Derived Macrophages

To obtain murine primary macrophages, mice of desired genotype were sacrificed as described above and disinfected with 70 % ethanol. To isolate the bone marrow, the legs were cut off and all muscles and connective tissue of both femora and tibiae were removed. The blank bones of each mouse were stored in PBS on ice and further processed directly after bone isolation of all mice was finished.

To avoid contamination with living cells on the outer side of the bones, they were placed for 3 min in 70 % ethanol and immediately transferred into fresh PBS.

The epiphyses of the bone were cut off and the bone marrow was rinsed with VLE DMEM with 10 % FCS. The four bones of each mouse were pooled and kept on ice.

All bone marrow suspensions were centrifuged for 5 min at 400 x g at 4 °C, followed by lysis of RBCs with 1 mL BMDM lysis buffer for 2 min. The lysis was stopped by addition of 2 mL BMDM medium, and cells were again centrifuged.

To remove cell aggregates or bone splinters, resuspended cells were filtered through a 70 µm cell strainer and transferred into two T175 flasks per mouse in 25 mL BMDM medium. This medium contains additional 0.1 v/v % β-mercaptoethanol and 10 v/v % filtered L929-conditioned medium. L929 cells secrete macrophage colony-stimulating factor (M-CSF) that induces the differentiation of bone marrow cells into macrophages.

After 7 days at 37 °C, the cells were washed with PBS and additional 20 mL PBS were added per flask. After incubation for 20 min at 4 °C, most of the cells were detached due to the missing Ca^{2+} ions in PBS. The remaining cells were gently removed with a cell scraper and all cells were centrifuged at 400 x g for 5 min at 4 °C, followed by resuspension in medium and seeding on plates in desired density.

2.2.7 *Ex Vivo* Analysis of T cells

To estimate the number of virus specific T cells, two different methods were used. The tetramer staining allows the quantification of circulating antigen specific T cells in the blood, several measurements can be done in the same experiment, giving a kinetic of the T cell response. The T cell restimulation with a specific peptide offers higher variability in the choice of antigen and is useful for the detection of memory T cell responses after an infection was controlled.

2.2.7.1 Tetramer Staining

For the tetramer staining 20 µL of whole blood were transferred into FACS buffer. In the next step, an GP-TET labeled with allophycocyanin (APC) was added and incubated for 15 min at 37 °C. This refers to a tetramer of four biotinylated H-2D^b molecules, the murine MHC class I, coupled by an APC-labeled streptavidin. Additionally, the MHC-I molecules were previously loaded with the GP33 (*KAVYNFATM*).

After tetramer binding, samples were stained for CD8 with a PE-Cy7 labeled antibody for 20 min at 4 °C to detect the CTL population during FACS analysis. FACS beads were added to allow an absolute quantification of cells.

Finally, the red blood cells were lysed with 1 mL BD FACS Lysing Solution by hypotonic lysis and simultaneously fixed with formalin for 7 min. After addition of 2 mL FACS buffer, the samples were centrifuged at 400 x g for 5 min at 4 °C and the supernatant aspired. The samples were recorded with a LSRFortessa cytometer and analyzed as described in 2.2.8 Flow Cytometry.

2.2.7.2 Restimulation of Splenocytes

To obtain the number of memory T cells responsive against LCMV, splenocytes of a mouse, that already controlled the infection after 30 days, were restimulated with different viral peptides and analyzed for induction of IFNγ or TNFα production.

Mice were killed, and spleens were harvested as described in 2.2.6.7 Sacrifice and Section of Mice. Spleens were transferred into PBS and smashed through a 70 µm cell strainer to obtain a single cell suspension and transferred into a 96-well plate, one well for each peptide and one unstimulated control. The cells were washed with PBS by centrifugation and supernatant aspiration and resuspended in DMEM with 2 % FCS containing the indicated peptide at 1 µg/mL. After 1 h at 37 °C, Brefeldin A was added to a final concentration of 10 µg/mL to each well, and cells were incubated overnight in the incubator.

The next morning, cells were pelleted and the surface antigens CD4 and CD8 were stained with αCD4-PE and αCD8-PE-Cy7 antibodies in FACS buffer for 20 min at 4 °C. After washing with

FACS buffer, the cells were fixed with 2 % Formalin in PBS for 15 min and washed again. The staining of the intracellular cytokines IFNγ and TNFα was performed in FACS Perm Buffer for 30 min. After washing, the samples were transferred into FACS tubes and measured with LSRFortessa cytometer.

2.2.8 Flow Cytometry

The samples were stained depending on the assay and measured with a LSRFortessa cytometer, harboring 4 excitation lasers, Violet (405 nm), Blue (488 nm), Yellow-Green (561 nm) and Red (640 nm), using FACSDiva software (both Becton Dickinson).

To setup the device, the voltage for each channel was set to a value that allows a discrimination between negative and positive at ~10^3 fluorescence intensity on 5 log scale. In a next step, all fluorescent channels were plotted against each other, and a compensation was set to overcome the spectral overlap of used dyes.

Data was exported as .fcs files and detailed analysis was performed with FlowJo 7.6.5. After exclusion of debris and doublets, the cells were further analyzed by their fluorescence intensities depending on the specific experimental design.

2.2.9 Immunofluorescence Imaging

Immunofluorescent images of organs were achieved by fluorescent staining of cryo-cut mouse tissues.

Therefore, flash-frozen organ samples, embedded in TissueTek medium were placed in a cryotome (Leica CM3050 S) and allowed to anneal temperature to -18 °C, which reduced the brittleness and made the still frozen blocks cuttable. 6 µm thick sections were cut and transferred in duplicate to microscopy glass slides and air dried for 20 min. Afterwards, samples were either placed at 4 °C in the dark for later use or directly processed for staining.

First, samples were fixed in acetone for 10 min. To avoid the aqueous staining solutions to flow off the slide, the sections were surrounded with a fat pen. To block unspecific binding sites, the slides were incubated for 10 min in Histology Staining Buffer followed by antibody staining steps for each 1 h in the dark with washing with Histology Staining Buffer in between. After the last washing step, one drop of Dako Fluorescent Mounting Medium was added to each slide, and they were covered with a coverslip.

When the mounting medium was dried, the slides were viewed with a Keyence BZ-9000 fluorescence microscope.

2.2.10 IFNα ELISA

The serum levels of IFNα were measured with an ELISA kit form ThermoFisher according to manufacturer's instructions. In brief, provided standards and prediluted serum samples were transferred to the provided microplate coated with a capture-antibody against IFNα. After 2 h incubation with a biotinylated detection antibody while shaking, the plate was washed and incubated with streptavidin-HRP for 1 h while shaking. The plate was again washed, followed by 30 min incubation with the provided TMB substrate solution until the highest standard turned dark blue. To stop the reaction, acid stopping solution was added, turning the blue color into yellow.

Finally, absorbance at 450 nm was measured with a Biotek Cytation 1 plate imager. A standard curve was constructed, and sample values were calculated based on it.

2.2.11 Measurement of LDH, ALAT and ASAT

The assess the serum levels of LDH, ALAT, and ASAT, 30 µL of sample was diluted 1:10 in PBS and analyzed by the central laboratory of the University clinic Essen.

2.2.12 Statistical analysis

Data presentation and statistical analysis was performed with GraphPad version 7. If not mentioned differently, two-sided student's t-test was performed and a p-value < 0.05 was regarded as significant.

2.3 Software

All FACS analysis was done with FlowJo 7.6.5, Geneious Prime was used for sequencing analysis and sequence alignments.

For minor calculations and writing, current versions Microsoft Excel and Word were used, literature management was done by EndNote X9.

PyMol was used for visualization and rendering of 3D-models.

2.4 Hardware

2.4.1 Devices

Table 10: devices

Device	Model	Use
Biological Safety Cabinet	ThermoFisher MSC Advantage	Protection against pathogens, ensuring sterile working conditions
Incubator	ThermoFisher Heracell 150i	Culture of mammalian cells
Centrifuge	Hettich Mikro 220R	Centrifugation of 1.5- and 2-mL tubes
Centrifuge	Eppendorf 5810R	Centrifugation of plates and 15- and 50-mL tubes
Thermocycler	AppliedBiosystem GeneAmp 9700	cDNA synthesis, PCR
qPCR Cycler	Roche LightCycler 480	qPCR
Flow Cytometer	BD LSRFortessa	Flow cytometric analysis of cells
Microscope	Keyence BZ-9000	Fluorescence imaging
Cryotome	Leica CM 3050 S	Cutting of tissue sections
TissueLyzer	Qiagen TissueLyzer II	Homogenization of organs
Plate reader	Biotek Cytation 1	Read-out of ELISA

2.4.2 Manual tools

Table 11: manual tools

Tool	Manufacturer	Use
Pipettes	VWR	Pipetting of liquids < 1.000 µL
Pipette controller	Hirschmann	Pipetting of liquids 1 – 25 mL
Castroviejo caliper	Fine Science Tools	Measurement of tumor size
Forceps	Fine Science Tools	Dissection of mice
Scissors	Fine Science Tools	Dissection of mice
Neubauer chamber	Carl Roth	Counting of cells

3. Results

3.1 Passage of LCMV-WE in H1975 Cells

To select for mutant viruses showing an enhanced replication, serial passage on H1975 cells, a human non-small cell lung cancer cell line, was performed as described in 2.2.3.1 Virus Passage.

The virus titer of each passage's supernatant was determined by focus-forming assay to ensure viral presence and estimate possible impacts on the replication capacity of the virus (Figure 7).

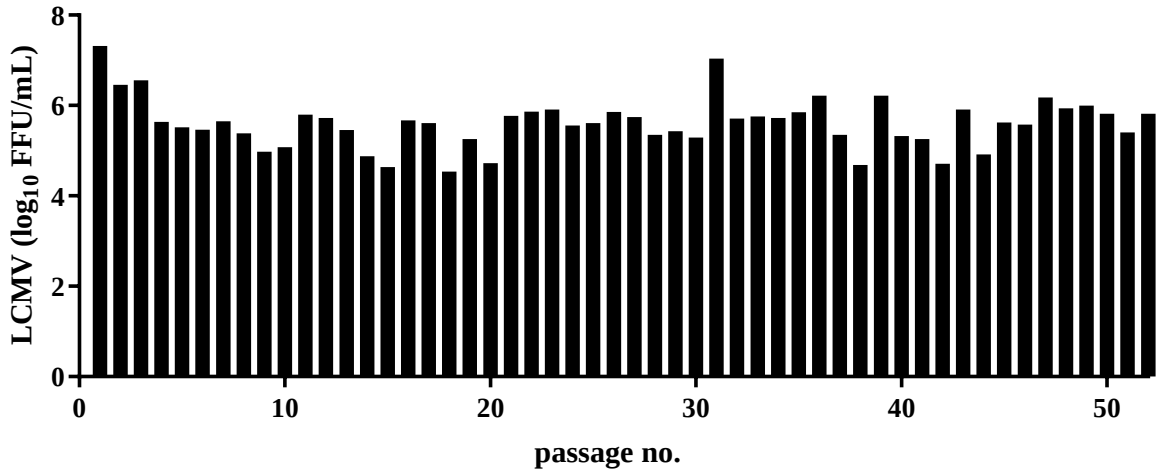

Figure 7: Viral titers of indicated passage number. The titer of every supernatant was afterwards determined by focu--forming assay. Almost constant titers between 10^5 and 10^6 FFU/mL were achieved, with an exception in the first passage and in passage 31.

During the passage, the viral titers of the supernatant after 72 hours were similar between 10^5 and 10^6 FFU/mL with only one exception in passage 31 and the first passage. Slight differences in cell culture conditions or the different MOIs at infection are possible explanations.

The virus-mutant present in the supernatant after 52 passages was named "P52" and sequencing was performed. Here, two mutations in the viral glycoprotein were revealed. The first mutation replaces the ATA codon by an ATG, resulting in an amino acid exchange at position 181 from isoleucine (I) to methionine (M). The second mutation at position 185 was AGG to TGG exchange, coding for a tryptophan (W) instead of an arginine (R), see Figure 8.

Figure 8: Sequence alignment of WE and P52 of the coding sequence for amino acids 180 - 186 of viral glycoprotein. LCMV mutant P52 harbors two mutations in the viral glycoprotein, I181M and R185W. Sequence alignment was created using Geneious Prime.

To test the stability of the virus, the passage was continued for additional 39 passages and after 91 passages in total, "P91" was generated. The viral titers of passage 53 to 91 were determined. Again, almost constant virus titers in passage supernatant were detectable (Figure 9).

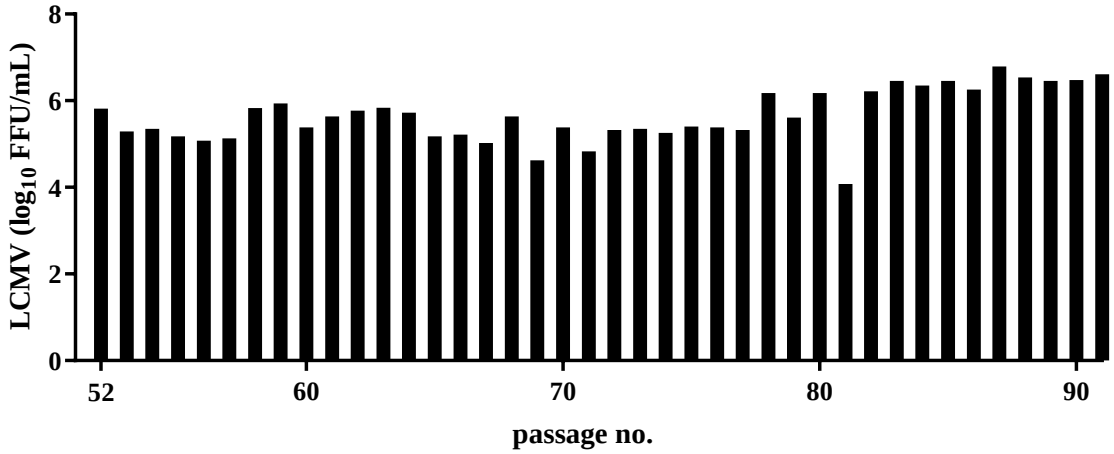

Figure 9: Viral titer of indicated passage numbers. The titer of each supernatant was afterwards quantified by focus-forming assay.

Sequencing of the virus generated in P91 revealed a S-segment identity of 100 % identity to the S-segment of P52 virus.

3.2 3D-structure of mutated LCMV-GP

To speculate about possible changes in viral phenotype, the 3D-structure of the viral glycoprotein was rendered. The crystal structure of the LCMV glycoprotein was published as a dimer of two GP (Hastie et al., 2016). This dimer is most likely a crystallizing artefact, because the two C-terminal GP2, which contain many hydrophobic amino acids and seem to be located within the viral membrane, face in the opposite direction (see Figure 10). Secondly, crosslinking of LCMV GP clearly indicates trimeric organization of the mature protein complex (Eschli et al., 2006).

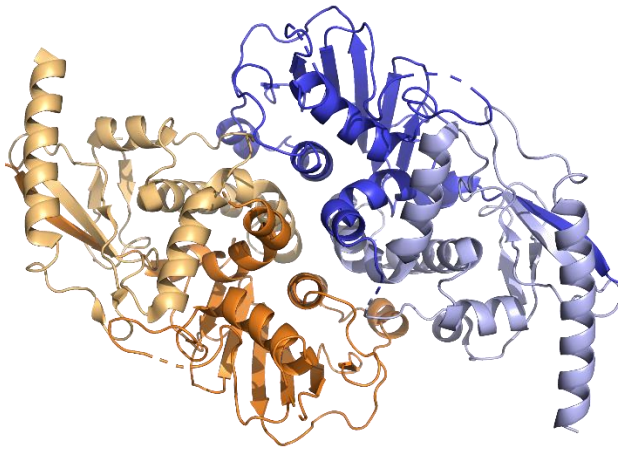

Figure 10: Crystal structure of LCMV GP. Dimer of two LCMV glycoproteins (blue and orange) after crystallizing. The GP2 subunits (light colored) face to the opposite direction, making this structure unlikely. Model is a re-colored version of PDB accession number 5ine, published by Hastie et al., 2016.

To get an idea of the real trimeric structure, a published 3D-structure of LASV GP bound by neutralizing antibodies was used (Hastie et al., 2017), see Figure 11. Due to the close relationship of LCMV and LASV and the use of the same cellular receptor, structural similarity of the glycoproteins was assumed.

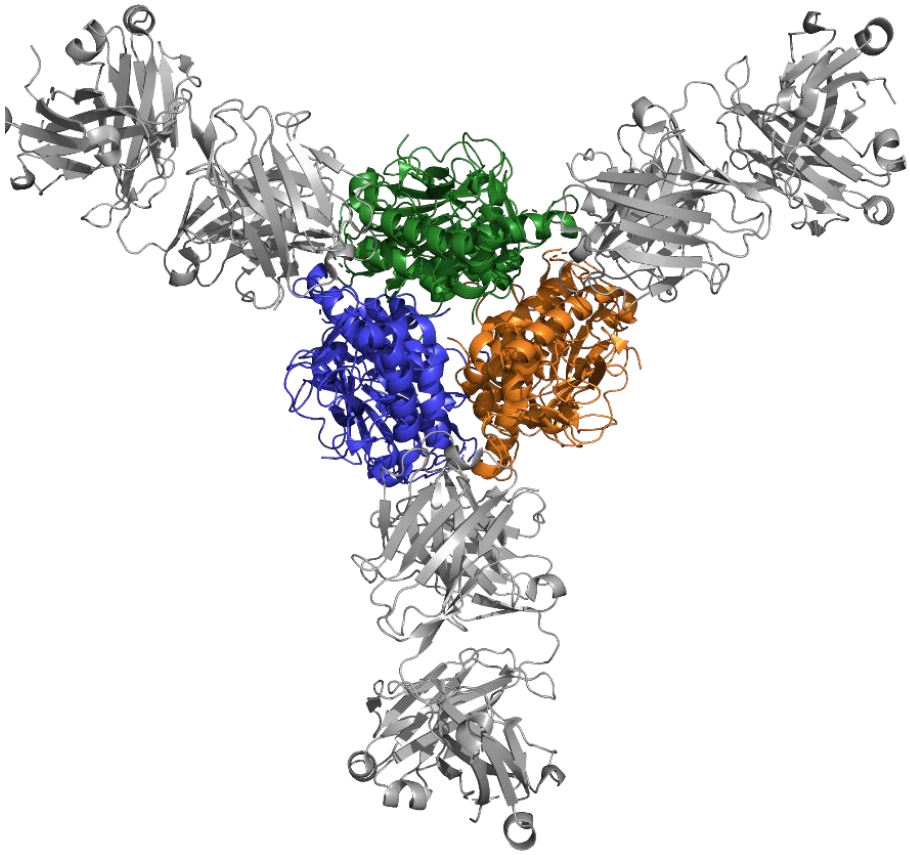

Figure 11: Structure of LASV GP, bound by neutralizing antibodies. Trimeric LASV GP (blue, orange, and green) are neutralized by three human antibodies (grey). Model is a re-colored version of PDB accession number 5vk2, published by Hastie et al., 2017.

Alignment of three LCMV GP monomers to the LASV GP trimeric structure gave an estimation of the expected LCMV GP trimer. Here, the position of amino acids 181 and 185 were visualized in Figure 12.

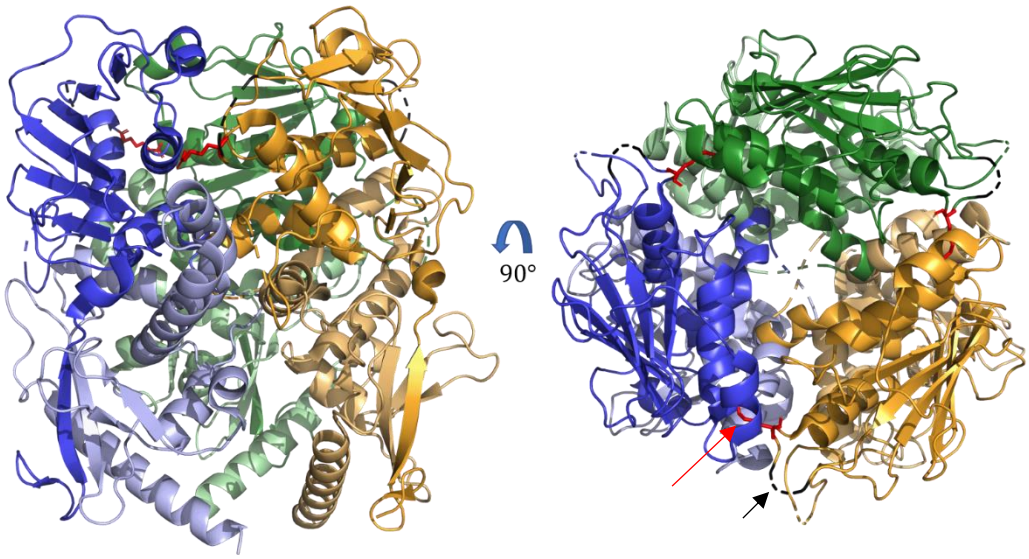

Figure 12: LCMV GP. Side and top view of estimated LCVM GP trimer. The monomers are colored in blue, orange and green, the GP2 subunit in light colors. The mutated amino acids in position 181 (loop 2, black) and 185 (red) are highlighted. The structure was calculated based on 5ine and 5vk2 as described above.

Both mutated positions are facing the outside of the mature glycoprotein, close to the receptor binding site at the top of the complex. This makes a change in receptor binding and cell entry possible.

3.3 Generation of Single-Mutant Viruses

Due to the presence of two amino acid exchanges, it was not possible to attribute phenotypical changes to one amino acid. To overcome this, older passages were also sequenced to identify a virus, carrying only one of these mutations (Figure 14).

Some particles show the wildtype sequence, while some particles had one or two mutations. As the read-out of Sanger sequencings is the consensus sequence of the templates, it usually gives clear peaks in the fluorescence curves, but in the presence of two quasi species, the curves overlap like shown in Figure 13.

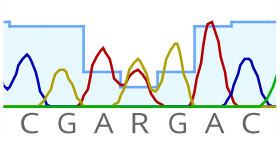

Figure 13: Example for double peak, indicating quasi species. A double peak for A (red) and G (yellow) is seen, showing that some viruses carry the wildtype G and some the mutated A (R = A or G).

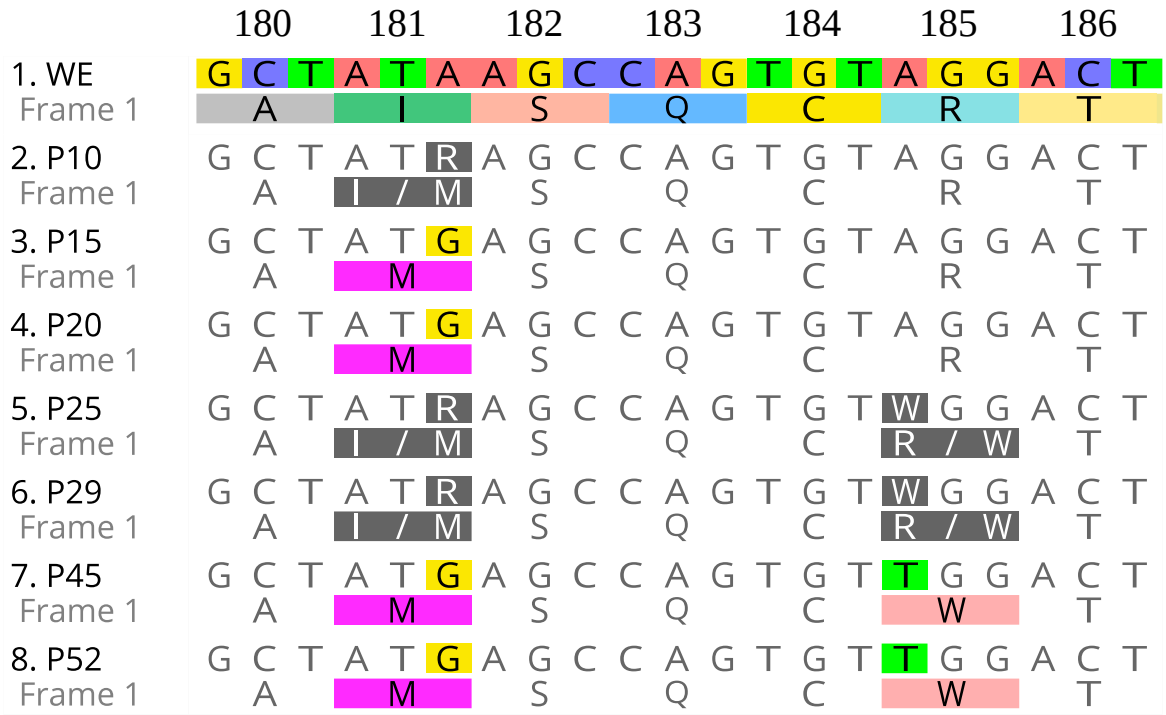

Figure 14: Sequence alignment of earlier passages. Earlier passages were sequenced, and history of mutations became visible. In P10, P25 and P29 the sequencing gave two results at the indicated positions, indicating the presence of different subpopulations, carrying either the mutation or being wildtype.

Figure 14 shows the presence of the acquired mutations is earlier passages. The mutation at position 181 occurred earlier, being already detectable in P10 and dominant from P15. In P29, both positions, 181 and 185, are present in wildtype and mutated constellation. Later passages only showed double mutated viruses. Therefore, passage 29 was subcloned to obtain the single mutants.

After limiting dilution of P29, eight subclones were sequenced to identify viruses bearing only one mutation in either position 181 or 185. Some subclones still showed sequencing results for more than one mutation, which might be due to insufficient dilution, but at least one subclone was found to harbor only one mutation in the viral glycoprotein gene (Figure 15).

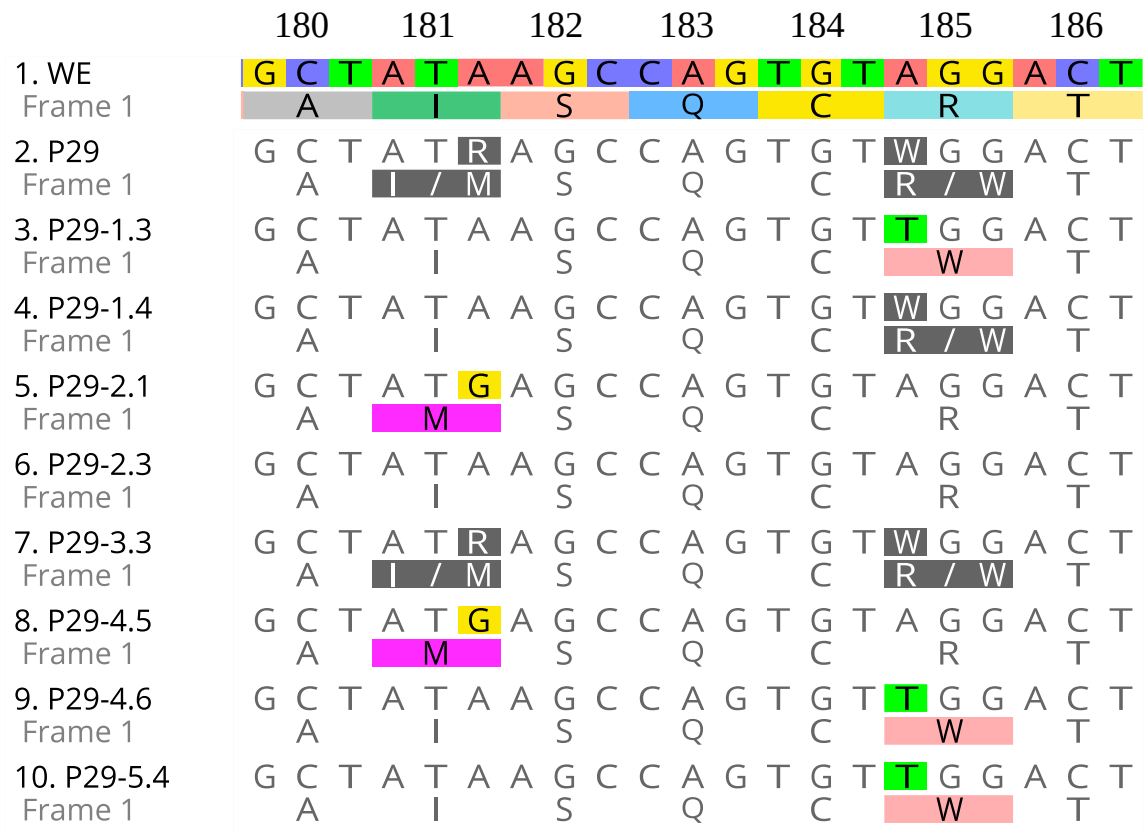

Figure 15: Sequence alignment of P29 subclones. Eight subclones, that contained virus, proven by focus-forming assay, were sequenced. Some of them still show quasi species, but both mutations are found to be unique in at least one subclone.

Sequencing of the selected eight clones proved the presence of different viruses in P29. Some of the subclones still show ambiguous results, indicating a not successful limiting dilution, but five subclones express solely one of the desired mutations. For all further experiments, P29-2.1 and P29-1.3 were used as single-mutants for I181M and R185W respectively and compared to wildtype WE and double-mutant P52.

3.4 *In Vitro* Replication of Mutant Viruses

To assess replication capability of viruses *in vitro*, three human cancer cell lines were infected with different MOI and supernatant was analyzed by focus-forming assay at different timepoints (see Figure 16).

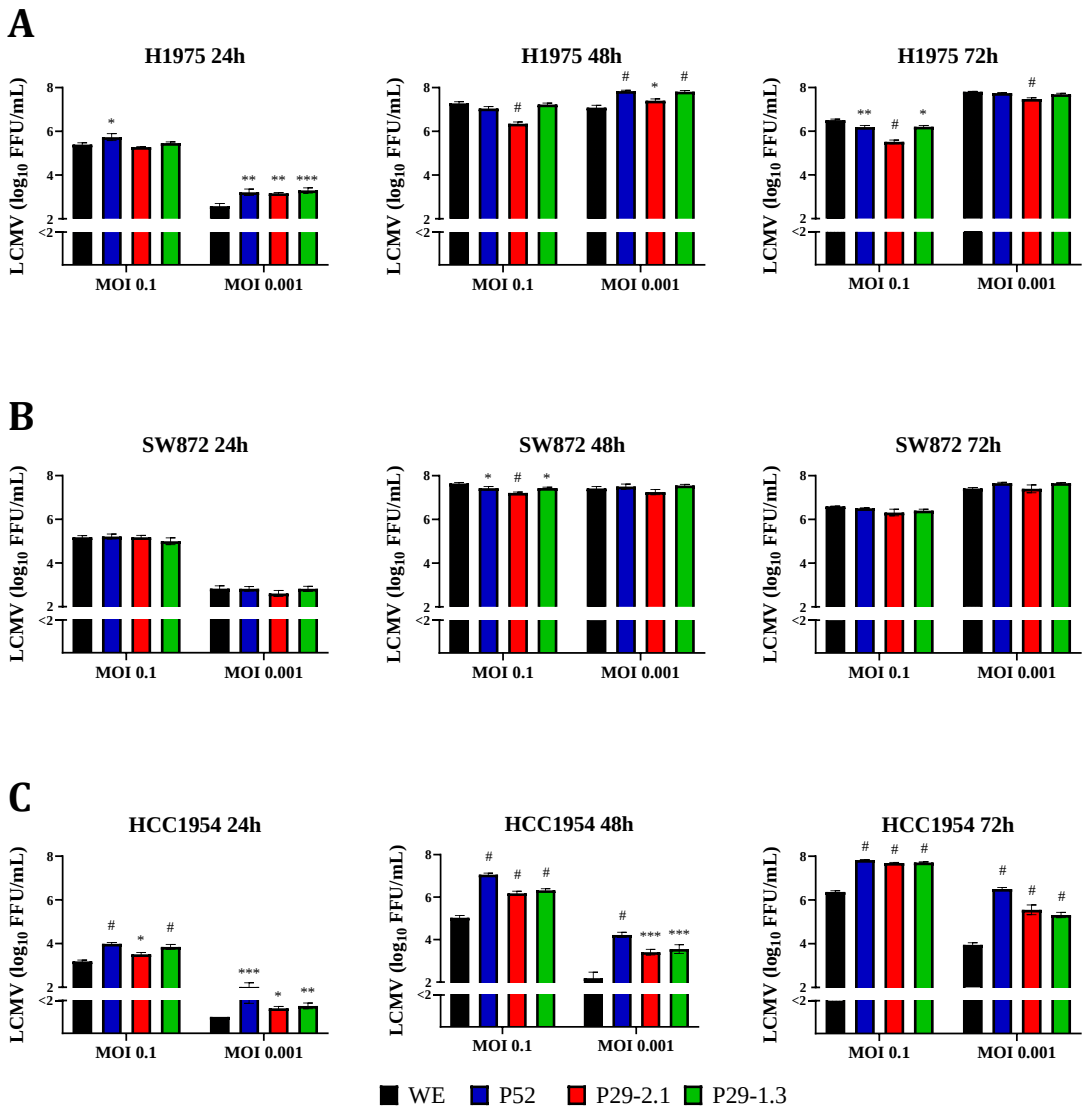

*Figure 16: Replication capability in vitro. Human cancer cell lines H1975 (A), SW872 (B) and HCC1954 (C) were infected with different MOI and infectious titer in supernatant was determined by focus-forming assay. Statistical analysis was done by One-way ANOVA with symbols indicating p-value in comparison to WE. *: p<0.05, **: p<0.01, ***: p<0.001, #: p<0.0001, n = 6.*

All mutant viruses show significant differences in their replication on the tested cell lines compared to the replication of LCMV-WE. On H1975 cells, the cells used for the generation of the viruses, P52 shows slightly increased titers after 24 h with a MOI of 0.1 but significantly higher titers after infection with MOI 0.001 after 24 and 48 hours. After 72 hours, replication of LCMV-WE reaches same or even higher titers than the mutant viruses. At early timepoints, the two single mutations are equivalent to the double-mutated whereas after 48 h, P29-1.3 resembles the P52 phenotype in H1975 cells.

While the mutant viruses show almost no relevant differences on SW872 cells, the titers of are increased at all measured timepoints and MOI compared to WE. Except for the infection with

MOI 0.1 after 72 h, P52 additionally shows elevated replication capacity than both single-mutated viruses.

3.5 *In Vivo* Replication of LCMV-P52

To obtain an overview of the replication capacity *in vivo*, C57BL/6 mice were infected with 2 x 10^4 FFU of LCMV-WE or P52 i.v. and virus distribution in spleen on day 1 and 3 after infection was observed. The viral titers in spleen determined by focus-forming assay gave no significant differences (Figure 17).

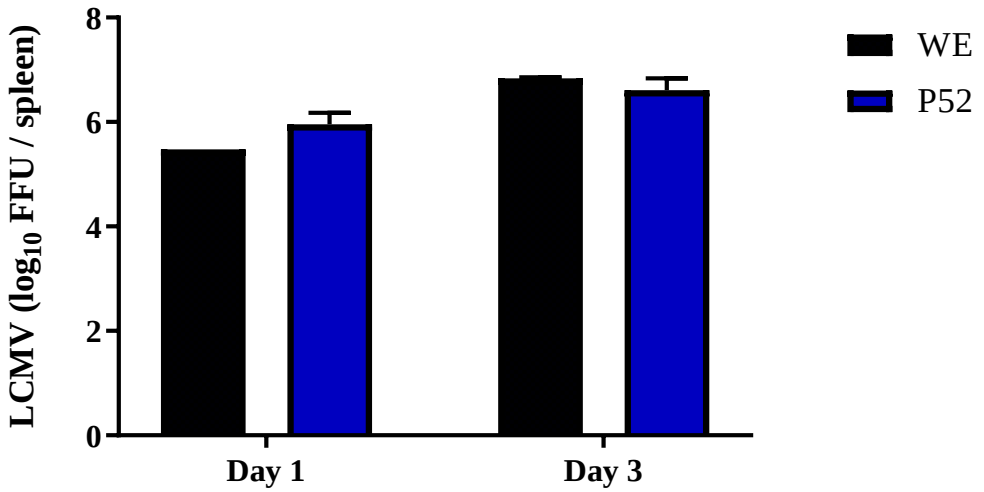

Figure 17: Virus titers in spleen. C57BL/6 mice intravenously infected with 2 x 10^4 FFU of indicated virus were sacrificed on day 1 or 3, and virus titer in spleen was determined by focus-forming assay. (n = 3)

To get a more detailed view on the splenic distribution of the virus, immunofluorescent staining of tissue sections was performed. In line with published data (Honke et al., 2017), the infection with 2 x 10^4 FFU of LCMV-WE resulted in only few infected cells, mainly being $CD169^+$ marginal zone (MZ) macrophages after one day of infection (Figure 18, A). LCMV-P52 shows the same distribution pattern to $CD169^+$ cells but can be detected in the majority of those cells. Three days after infection, the MZ architecture is partially lost, and the viruses spread into the red and white pulp. Whereas red pulp infection by LCMV strain WE was rarely visible, NP expression could be observed in almost entire spleen tissue after P52 infection (Figure 18, B).

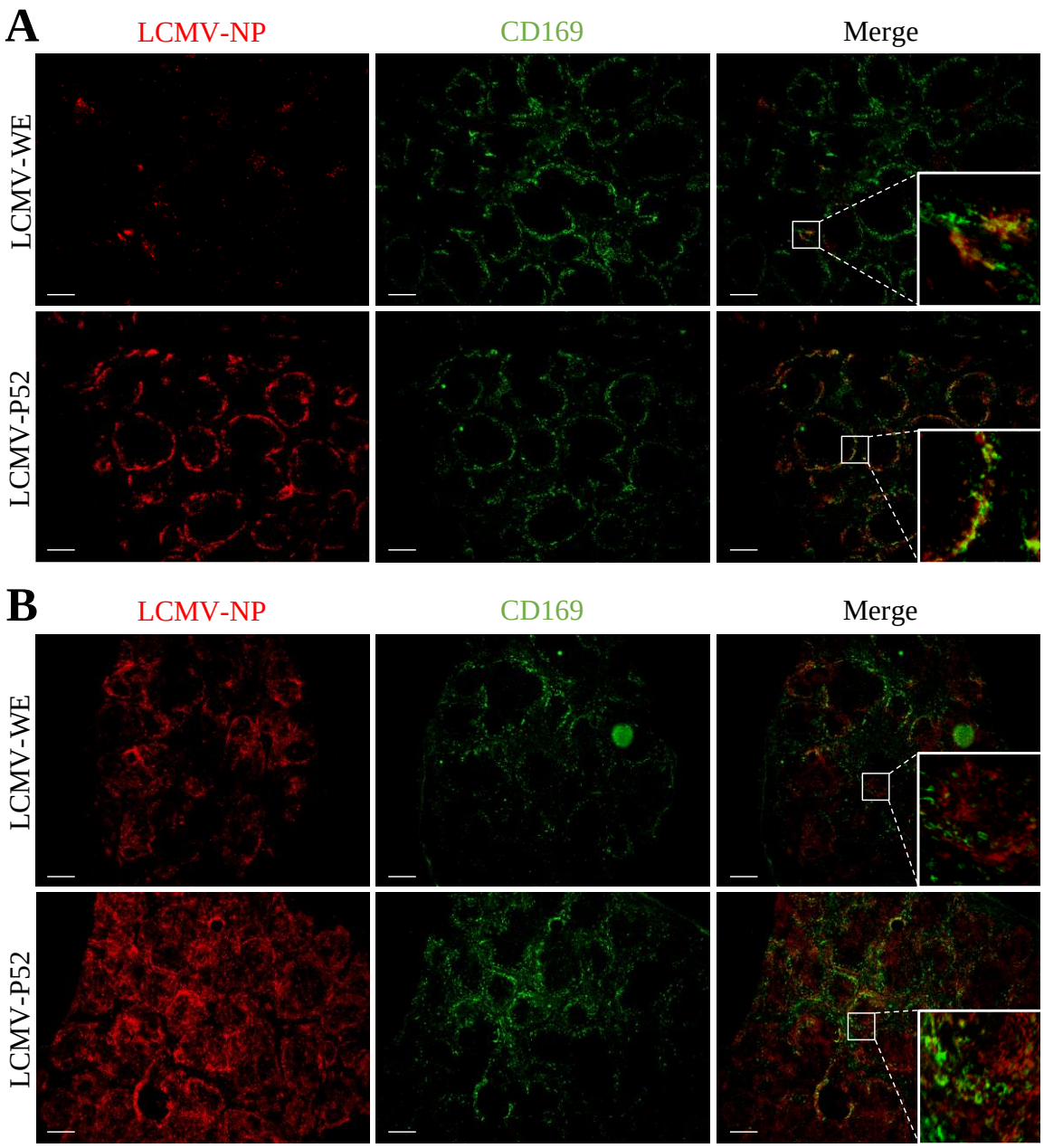

*Figure 18: Immunofluorescent staining of spleen sections. C57BL/6 mice were infected with 2 x 10^4 FFU of LCMV-WE or LCMV-P52 i.v. and spleens of infected mice were stained for LCMV-NP (red) and CD169 (green) on day 1 (**A**) and day 3 (**B**) after infection. Scale bars, 200 µm.*

To investigate whether the mutations lead to a persistent infection, mice were sacrificed on day 30 and LCMV target organs were analyzed by focus-forming assay.

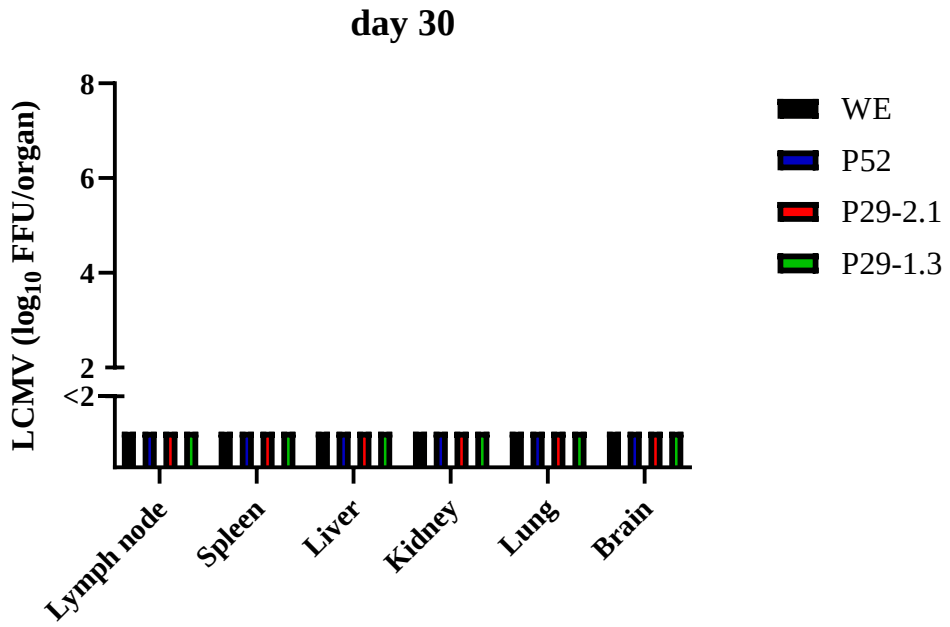

Figure 19: Organ titers on day 30. C57BL/6 mice infected with 2 x 10^4 FFU of indicated virus were sacrificed on day 30 and organ titers were determined by focus-forming assay.

No infectious particles were detectable in all organs tested (Figure 19).

3.6 Innate Immune Response

3.6.1 IFN-I

Type I interferon is a common marker for innate immune activation after systemic infection with viral pathogens. For this purpose, C57BL/6 mice were infected with 2 x 10^4 FFU i.v. of each virus strain and serum IFNα levels were determined by ELISA after 6, 12, 24, 48 and 72 h (Figure 20).

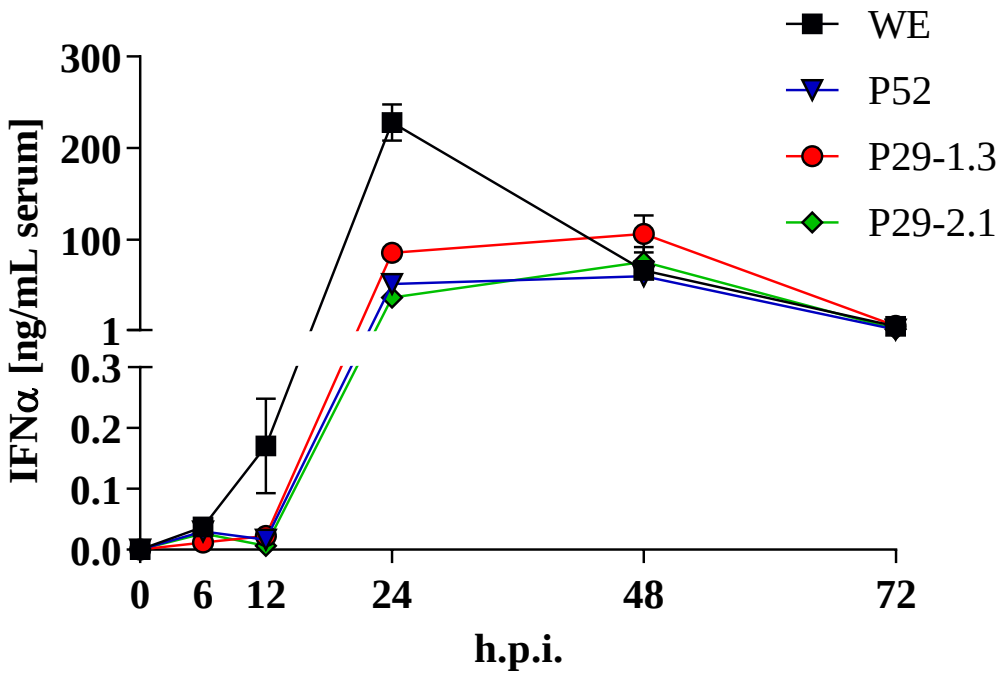

Figure 20: Serum IFNα levels at indicated time points. Mice were bled 6, 12, 24, 48 and 72 hours post infection (h.p.i.), and IFNα levels were measured by ELISA. For 6 and 12 h, n = 3, for all other time points n = 6.

All mutant strains showed reduced IFNα levels after 12 and 24 h compared to the wildtype LCMV strain WE, while being comparable after 48 and 72 h.

3.6.2 TLR2

Some arenaviruses like Junín virus (JUNV), but also some LCMV strains like Armstrong are known to induce innate immune response by stimulation of TLR2-TLR6-dimer (TLR2/6) (Hayes et al., 2012). The two mutations are located on the outer side of the glycoprotein structure and might therefore be detected differently by TLR2/6.

For this purpose, bone marrow-derived macrophages (BMDM) from wildtype (WT), *Tlr2*$^{-/-}$ and *Myd88*$^{-/-}$.*Trif*$^{-/-}$.*Cardif*$^{-/-}$ mice were stimulated with 1 x 10^9 FFU LCMV directly or after virus inactivation by UV exposure. The expression of TLR2-induced genes after two hours was analyzed by RT-qPCR (Figure 21).

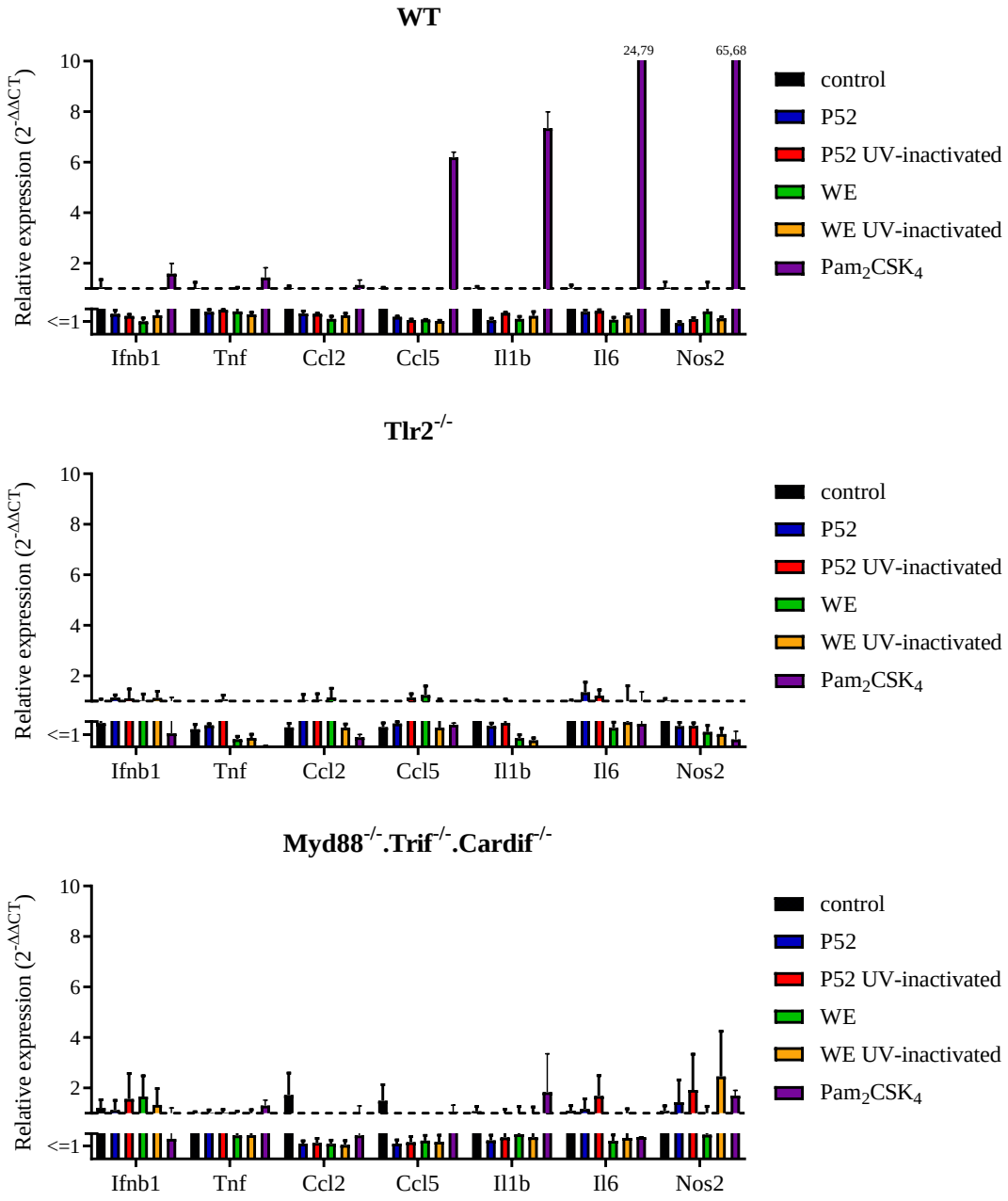

Figure 21: WE and P52 do not induce cytokine expression in BMDM via TLR2. BMDM of different genotypes were stimulated with live or UV-inactivated virus or TLR2/6 agonist Pam_2CSK_4 for 2 hours. Cytokine expression was measured by RT-qPCR and normalized to Gapdh expression. (n = 6)

Neither WE nor P52 induced cytokine expression in BMDM, whereas the TLR2/6 agonist Pam_2CSK_4 confirmed the ability of WT BMDM to respond to TLR2 activation. The panel of cytokines used for this assay was chosen according to prior publications about TLR2 stimulation (Cuevas & Ross, 2014; S. Zhou et al., 2005) and showed significant induction after Pam_2CSK_4 administration.

3.7 Adaptive Immune Response

3.7.1 CD8$^+$ T cells

To measure the CD8$^+$ T cell response after LCMV infection, the frequency of virus specific CD8$^+$ T cells in the blood can be used as a surrogate marker and is determined by a tetramer staining on day 8, 10, 12 and 14 after infection.

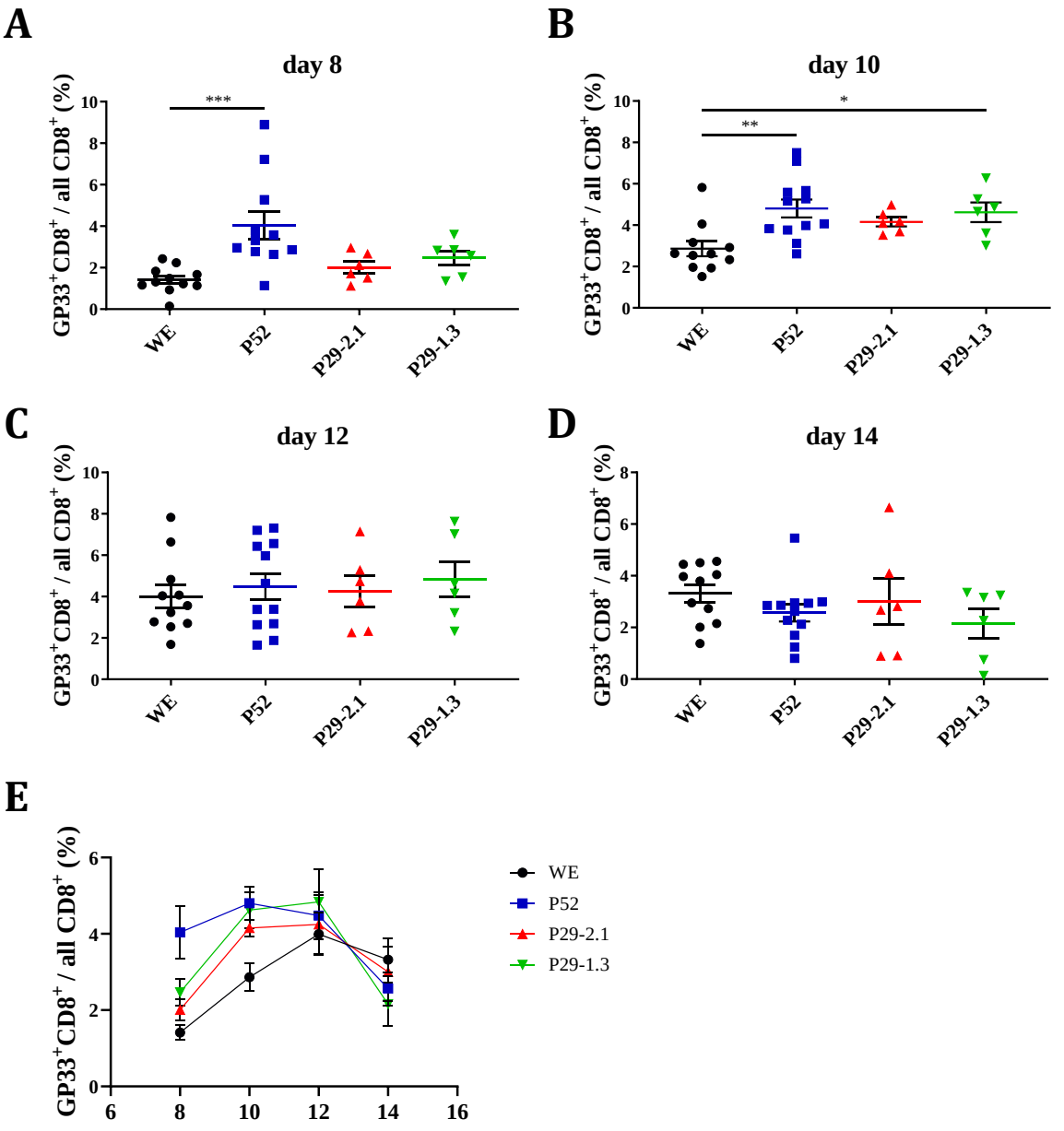

*Figure 22: P52 elicits a faster T cell response with higher frequencies on day 8 and 10. Blood samples of C57BL/6 mice infected with 2 x 10^4 FFU of indicated virus were assessed for GP33-specific T cells on day 8, 10, 12, and 14 (A-D). Graph E shows the above data over time. Statistical analysis was done by One-way ANOVA with symbols indicating p-value in comparison to WE. *: p<0.05, **: p<0.01, ***: p<0.001, n = 6.*

In Figure 22, the frequencies of CD8$^+$ T cells specific for a viral epitope representing amino acids 33 - 41 of the viral glycoprotein (GP33) are shown. P52 induces a faster and stronger anti-viral

T cell response compared to WE, while P29-2.1 showed no difference and P29-1.3 only slightly increased the frequency on day 10.

3.7.2 Development of Memory T Cells

Acute infections with LCMV are usually controlled by WT mice within 10 - 20 days, depending on strain and dose. Afterwards persistence of memory T cells gives immunity against recurrent infections with LCMV. To measure these LCMV-reactive T cells, splenocytes were isolated on day 30 and restimulated with viral peptides. Those T cells that produce IFNγ or TNFα, are considered virus specific. The frequencies of virus specific $CD8^+$ T cells are shown in Figure 23.

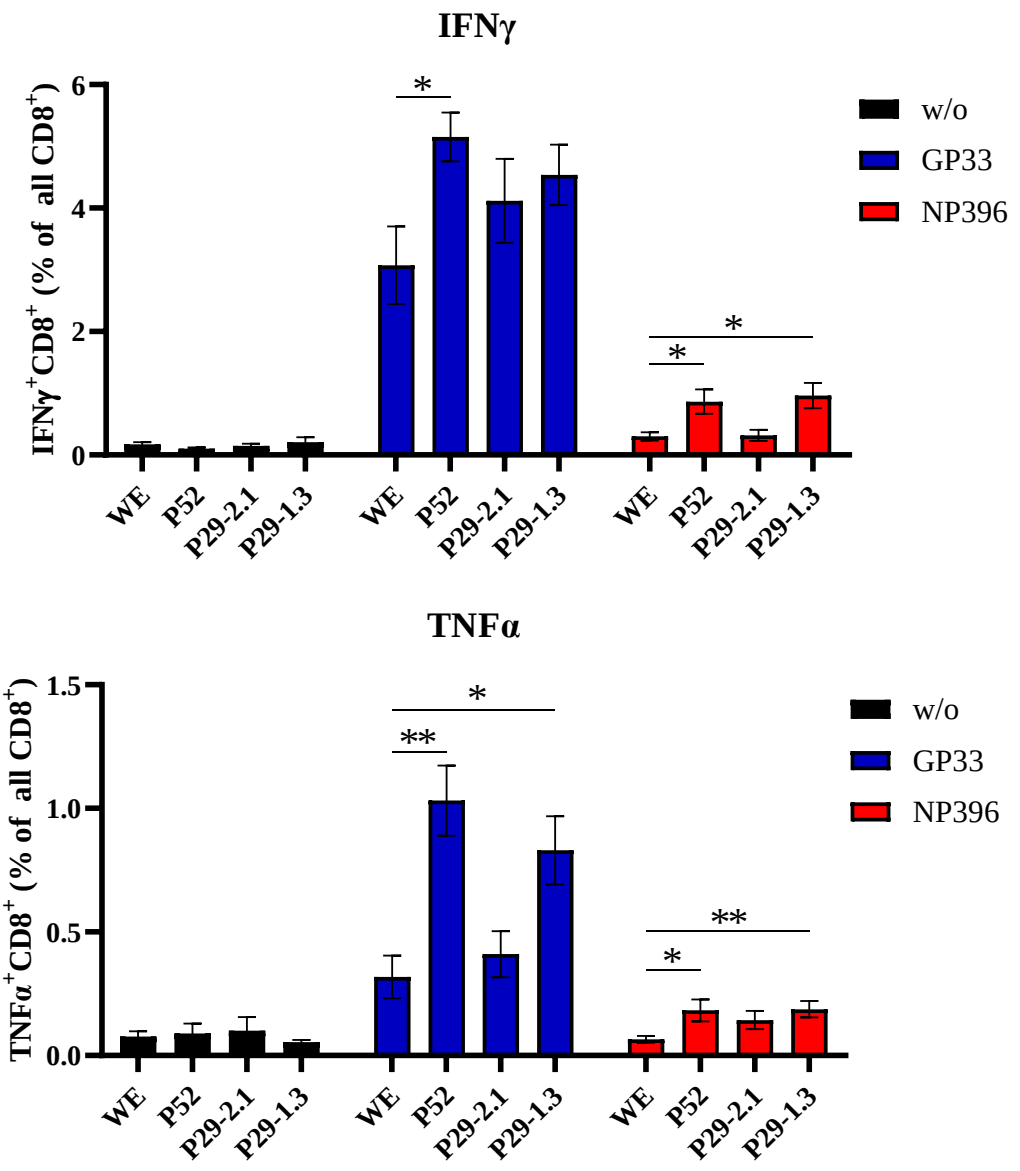

*Figure 23: Restimulation of splenocytes on day 30. Splenocytes were restimulated over night with the viral peptides GP33, NP396 or medium only. After 1 hour, BFA was added to inhibit secretion of cytokines. Statistical analysis was done by One-way ANOVA with symbols indicating p-value in comparison to WE. *: $p<0.05$, **: $p<0.01$.*

The intracellular cytokine staining (ICS) showed similar results to the tetramer staining. Again, P52 exhibits higher frequencies of virus specific $CD8^+$ T cells able to produce IFNγ or TNFα compared to WE. P29-2.1 did not show significant difference to WE, whereas P29-1.3 induced more NP396 specific T cells producing IFNγ after stimulation with viral peptide.

The same increase is also seen in TNFα secreting T cells, further underlining the stronger T cell induction by P52.

3.7.3 Neutralizing Antibody Response

To investigate if the changes in the viral glycoprotein also enhanced the B cell response and induced neutralizing antibodies, the sera of the same mice were analyzed for nAb.

Neither WE nor the mutant viruses induced measurable nAb titers within the observation period of 30 days as shown in Figure 24.

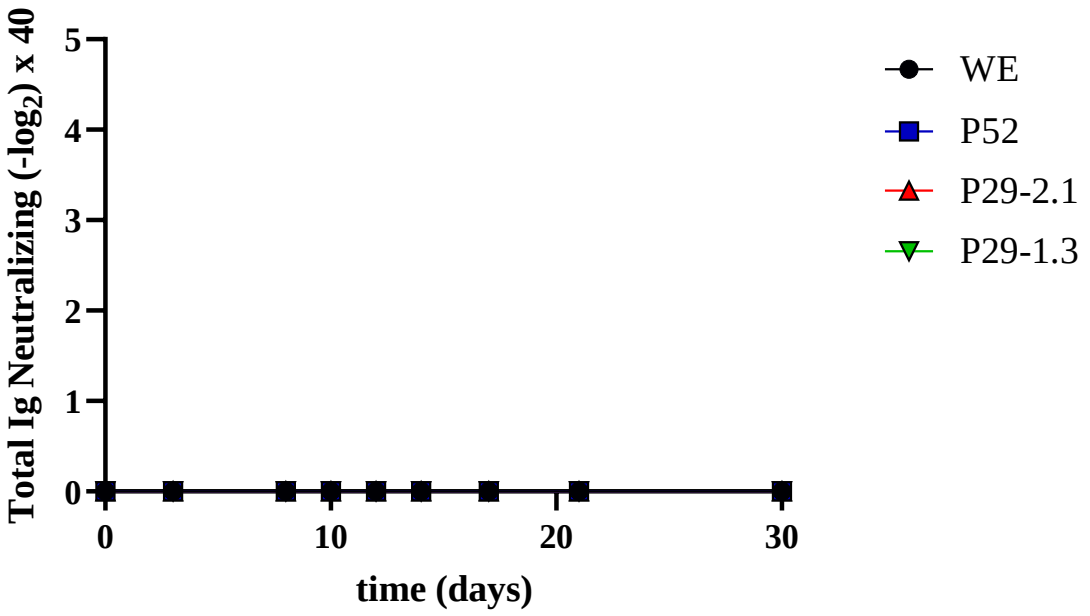

Figure 24: Total neutralizing Ig. Occurrence of neutralizing antibodies in the serum after infection with 2 x 10^4 FFU of indicated virus was measured at different timepoints.

3.8 Virus-Induced Hepatitis

The LCMV strain WE is used as a model for virus-induced transient hepatitis in mice (Beier et al., 2015). Infection with a high dose of LCMV-WE results in infection and consecutive T cell-mediated killing of hepatocytes, leading to increased levels of hepatic enzymes in the serum between day 8 and 10. To investigate possible changes in hepatic tropism of the mutant viruses, sera of infected mice were analyzed for lactate dehydrogenase (LDH), alanine aminotransferase (ALAT) and aspartate aminotransferase (ASAT) activity (Figure 25).

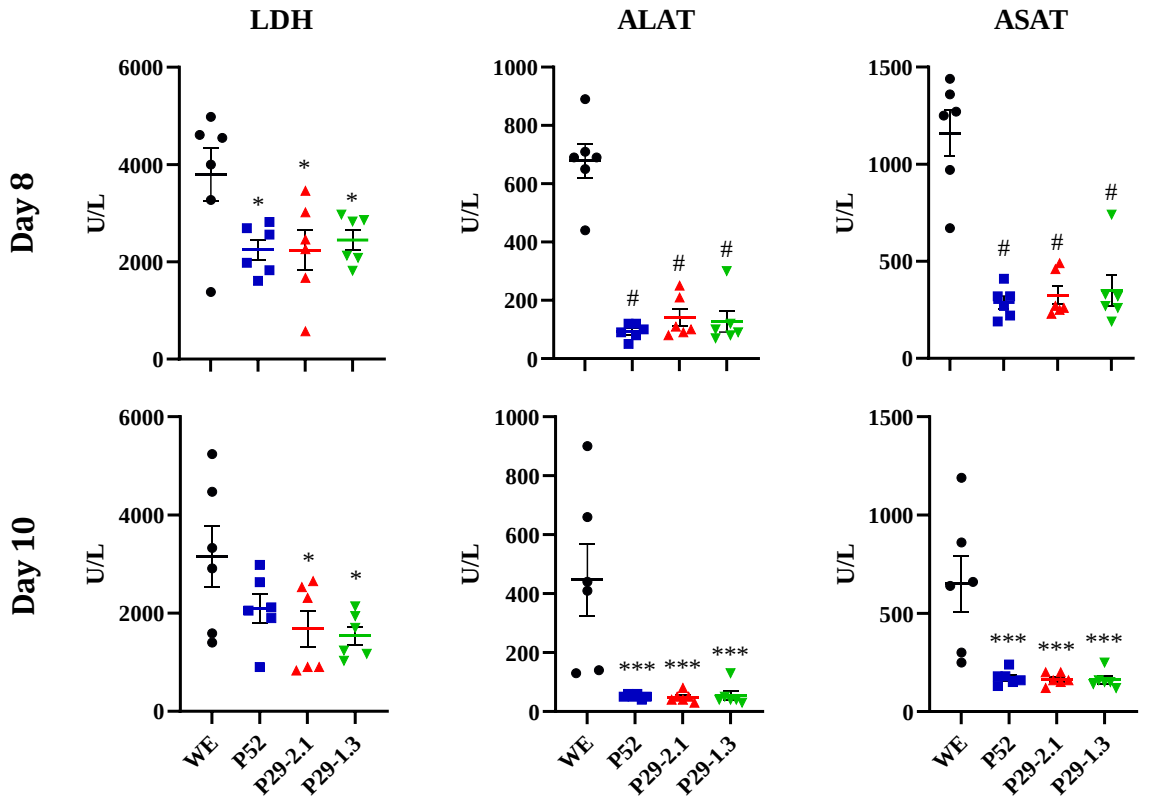

*Figure 25: Activity of hepatic enzymes in the serum. To assess the liver damage, serum activities of LDH, ALAT and ASAT were determined on day 8 and 10 of mice infected with 2 x 10^4 FFU i.v. of indicated virus. Statistical analysis was done by One-way ANOVA with symbols indicating p-value in comparison to WE. *: p<0.05, **: p<0.01, ***: p<0.001, #: p<0.0001.*

All three mutant viruses show clearly reduced levels of LDH, ALAT and ASAT on day 8 as well as day 10 after infection, indicating less infection and T cell mediated destruction of hepatocytes.

3.9 Tumor Growth Inhibition by Mutant Viruses

To assess whether these phenotypical changes of the virus *in vitro* and in naïve mice also impacts the anti-tumoral effect of LCMV *in vivo*, NOD.SCID mice bearing a subcutaneous human H1975 tumor were infected i.v. with 2 x 10^4 FFU of different LCMV mutant viruses and WE and tumor growth was observed (Figure 26).

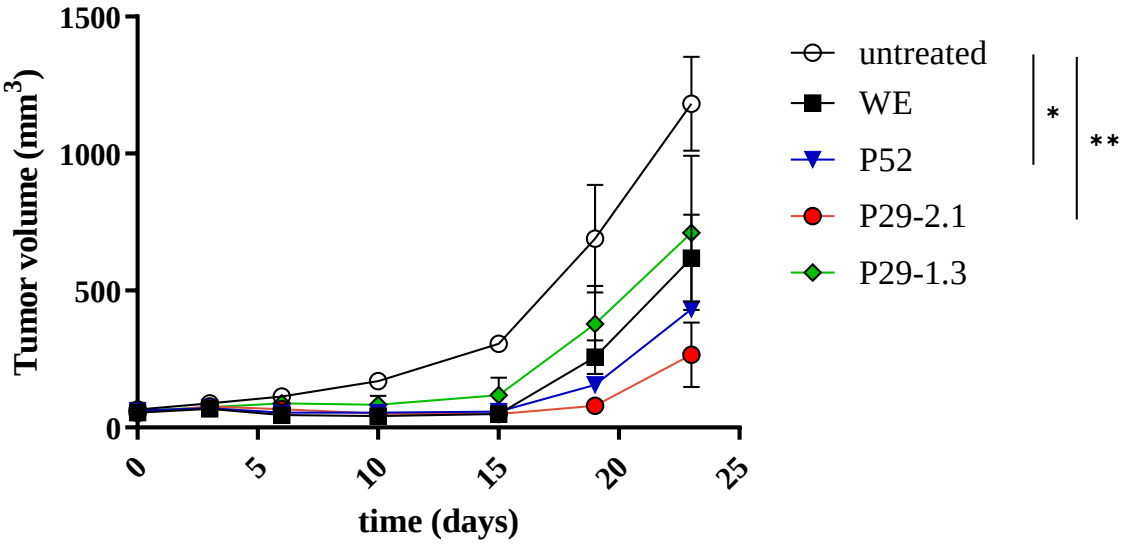

*Figure 26: Growth of H1975 tumors. 1 x 10^6 H1975 cells were injected on day -7 and mice were treated on day 0 with 2 x 10^4 FFU of indicated virus i.v. Statistical analysis was done by One-way ANOVA with symbols indicating p-value in comparison to untreated group on day 23. *: p<0.05, **: p<0.01.*

The H1975 cell line was used for this experiment, because the P52 was the result of a passage on this cell line and shows higher replication *in vitro*. Indeed, the P52 treated tumors showed slower growth than untreated or WE treated tumors. The role of the single mutations appears to be ambivalent. Together with P52, the P29-2.1 treated tumors are significantly smaller than the untreated tumors on day 23. The R185W mutation carried by P29-1.3 is not beneficial in the used model.

3.10 Combination Therapy with PD-1 Blockade

Nowadays, the combination of different drugs and modalities is standard in cancer treatment. The blockade of immune checkpoints like PD-1 or CTLA-4 are in use for many different cancer entities, but mostly in combination with classical chemotherapy.

To investigate if the virus immunotherapy also benefits from combination with checkpoint-inhibitors, immunocompetent C57BL/6 mice bearing B16-Ova melanoma were treated either with P52 or αPD-1 alone or in combination (Figure 27).

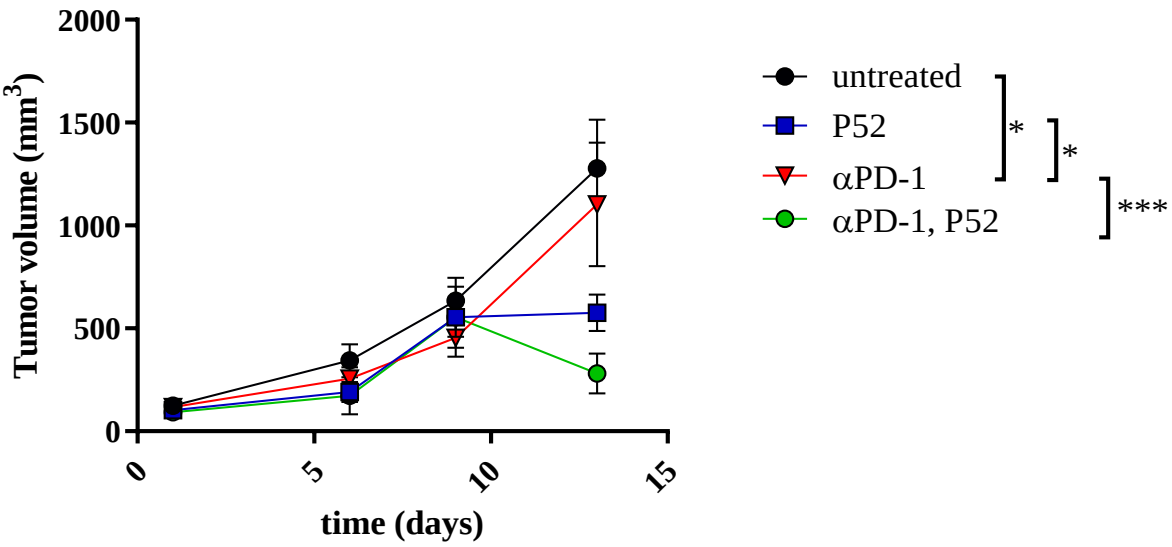

*Figure 27: Tumor growth of B16-Ova tumors after treatment with P52 and αPD-1. Immunocompetent C57BL/6 mice (n = 6 - 8 per group) were treated with αPD-1 blocking antibody, P52 or the combination. Statistical analysis was done by One-way ANOVA with symbols indicating p-value day 13. *: p<0.05, **: p<0.01, ***: p<0.001.*

The blocking of PD-1 had no significant effect on tumor growth when applied alone, whereas P52 was able to inhibit the tumor growth for the observation period. Interestingly, the combination of LCMV-P52 and PD-1 blockade even increased the anti-tumoral effect.

4. Discussion

4.1 Proof of Principle

It is widely known that serial passage of a virus can lead to its attenuation and thereby can create a safe vaccine (Eto et al., 2021; Whitehead et al., 1998). But before, it was not shown that induced change of tropism may also be used to improve the infection of malignant cells and consecutively enhance the anti-tumoral properties of a virotherapeutic agent.

Here, it was proven that passage-induced point mutations can enhance replication in tumor cells *in vitro* and can affect the innate and adaptive immune response *in vivo*. Together the anti-tumoral effect was slightly improved in H1975 xenograft model, and syngeneic B16-Ova tumors became responsive to PD-1 blockade.

The generation of P52, a virus showing clear phenotypical changes compared to the wildtype WE, proves the general possibility to manipulate viruses to become more effective as tumor-treating agent. From then, this technique was called “Fast Evolution Platform”.

Sequencing and subcloning results from earlier passages confirm a continuous development process. Both mutations were individually found in passage 29 together with double mutated viruses and wildtype particles. Comparable to classical evolution theory, different quasi-species are present next to each other until one of them turns out to be superior. 23 passages later, the dominant genotype, later called “P52”, was the only detectable species.

The fact that P52 was stable for additional 39 passages on H1975 cells proves the adaptation of the virus to the new environment. Furthermore, the enhanced replication not only in H1975 cells but also in HCC1954 cells representing another tumor entity shows the adaptation not only towards this special cell line but gives hints to a tropism change towards malignant cells in general.

4.2 Differences of WE and Mutant P52

Even little changes in amino acid sequence can impact the overall phenotype of a virus. Especially for LCMV, the two closely related strains Armstrong and its derivate Clone 13 show clear differences in infection characteristics *in vivo*. While the Armstrong strains exhibits a neurotropism with low affinity to α-DG, Clone 13 has high affinity to α-DG and shows a clear viscerotropism (Smelt et al., 2001). Nevertheless, the glycoproteins only differ in one amino acid that changes the protein folding and thereby explains the contrary binding affinities and tropisms (Zapata & Salvato, 2013).

This example shows that even minor differences in amino acid sequence can change the phenotype of an arenavirus like LCMV. Therefore, the new mutants were further characterized and compared to wildtype virus WE.

4.2.1 *In Vitro* Replication

The easiest way to characterize viral replication capability is the infection of cell lines *in vitro* and the determination of viral titers in the supernatant. To compare the mutant viruses to WE, a panel of three different human cancer cell lines was chosen, representing the generation cell line H1975, a human NSCLC cell line, HCC1954, an established model cell line for human breast cancer and SW872, a cell line isolated form human liposarcoma.

As both mutations were found in the viral GP1 that is responsible for the attachment to the cellular receptor, this gives rise to the hypothesis that the viral receptor binding or fusion is affected by the mutations. This is further supported by the 3D-model showing the proximity of the changed amino acids to each other and their localization on the protein surface. To prove this theory, two different MOI were used for the replication study. The lower the initial infectious dose, the more important the first replication cycle is for the virus titer after 24 hours. At later timepoints, the effect of the early binding or fusion might be covered by the comparable replication speed after fusion which is mainly depending on the viral replication complex and to a lesser extent by the GP.

Indeed, LCMV-WE reaches comparable or even slightly higher titers on H1975 cells when infected with MOI 0.1. But initial infection with low MOI of 0.001 gives significantly higher titers in all mutated viruses especially after 24 h, less after 48 h and finally a saturation after 72 h. This is exactly mirroring the hypothesis of low MOI and early timepoints being most likely different.

Another aspect of this experiment points at the role of the single mutations. On the generation cell line H1975, all mutated viruses show comparably enhanced viral titers after 24 h at low MOI. This indicates that both mutations are independently improving binding or fusion in H1975 cells.

Similar results were seen for HCC1954 cells. Additionally, a clear synergistic effect of both mutations is seen after 48 h. This enhanced replication in another tumor cell line indicates the generally increased replication of P52 and the other mutant viruses in human cancer cells.

4.2.2 *In vivo* Replication

To investigate if the mutations only increased the replication of the virus or indeed shifted the tropism from healthy to malignant cells, naïve mice were infected with WE and P52 and the virus replication in healthy spleens on day 1 and 3 was compared.

The total infectious titer was comparable with both viruses and the early distribution pattern within splenic tissue was also identically restricted to the marginal zone macrophages, although a higher number of MZ macrophages were infected by P52 at day 1. A persistence of the infection could also be excluded by negative organ titers 30 days after infection.

Concludingly, the replication in healthy tissue remains almost unaffected whereas the replication in tumor cells is increased by the two generated mutations. This implies a successful tropism change towards malignant cells.

4.2.3 Innate Immune Response

In contrast to oncolytic viruses that mainly act by infection and lysis of tumor cells, the effective treatment of tumors with LCMV relies on the activation of innate and adaptive immune responses. As a surrogate marker for early immune activation by viral infections, type I interferon levels in the serum were determined. Interestingly, WE had significantly higher levels of IFN-I after 24 h that equalized after 48 hours. Usually, the IFN-I levels correlate with the present virus as they depend also on the infectious dose (Stamm et al., 2012). This gives the hint, that the replication of P52 is actually reduced in healthy mice early after infection and the IFN peak is lower than for WE. This might be beneficial for later clinical use, because many of the observed early side effects of vaccinations and virotherapies are identical to those of treatment with recombinant IFN-I (Sleijfer et al., 2005).

To explain these differences, the different ways to induce IFN-I production were discussed. There are mainly two pathways to induce relevant amounts of IFN-I, either by intracellular RNA sensors like RIG-I or MDA-5 with mitochondrial antiviral-signaling protein (MAVS) as the shared signal transducer, or via membrane bound TLRs followed by activation of usually myeloid differentiation primary response 88 (MyD88) or TIR domain-containing adaptor-inducing interferon-β (TRIF) in the case of TLR3. As the serum IFN-I on day 2 strictly depends on MAVS, intracellular sensors seem to be important at that timepoint. But on day 1, MAVS $^{-/-}$ mice exhibit no difference to wildtype mice (S. Zhou et al., 2010). As consequence, the IFN-I found on day 1 is not induced by RIG-I or MDA-5 but by other pathways, most likely TLRs.

As the RNA components only differ in two nucleotides and the viral NP that is known to inhibit cellular IFN-I induction (Martínez-Sobrido et al., 2006; S. Zhou et al., 2010) is identical, the

only possible explanation would be the detection of the mutated protein itself. TLRs that are known to recognize LCMV mainly detect the RNA (Suprunenko & Hofer, 2019), while TLR2 is the only one able to detect proteins of some viruses and $TLR2^{-/-}$ mice showed reduced IFN-I bioactivity (S. Zhou et al., 2005).

Although TLR2 is mainly known to detect lipoteichoic acids from $gram^{+}$ bacteria, it can also respond to some viral proteins. This is published for HSV-1, and also arenaviruses like JUNV and LCMV strain Armstrong (Hayes et al., 2012). To evaluate possible TLR2-mediated responses to WE or P52, bone marrow-derived macrophages from wildtype or respective knock-out mice were differentiated *ex vivo* and treated with highly concentrated virus preparations that were partially UV-inactivated to ensure no RNA replication can trigger intracellular RNA sensors. To exclude possible contaminations by cellular debris from the production process, the infection volume was reduced to a minimum of 1 µL and supernatant from uninfected production cells were used as control. To reach the desired MOI of 3 in 1 µL, stocks from serum-free cultured HEK293 suspension cells were used. Additionally, these cells and stocks were extensively tested negative for mycoplasma contamination, as triacylated lipopeptides from mycoplasma are also known to stimulate TLR2.

Unfortunately, no stimulation of TLR2 could be observed by WE or P52, only the TLR2 agonist Pam_2CSK_4 gave positive results, confirming the expression of functional TLR2 on the used BMDM cells.

As most of the IFN-I in serum is produced by pDCs after viral infection (Jung et al., 2008), differential infection of these specialized cells could explain the difference in IFN-I levels.

2.2.4 Adaptive Immune Response

The adaptive immune response consists of two columns, the antibody, and the T cell response. Depending on the virus, the importance of the columns differs greatly in concerns of immune response and viral clearance.

LCMV strains causing an acute infection like WE are known to be a strong inducer of $CD8^{+}$ T cell responses, whereas neutralizing antibodies are found rarely in mice due to the glycan shields of the viral glycoprotein (Sommerstein et al., 2015).

To evaluate the kinetic of the virus-specific T cells, the $CD8^{+}$ T cells raised against the dominant viral GP33 epitope were measured between day 8 and 14 after infection. Especially at early timepoints, P52 induced significantly higher frequencies of virus-specific T cells, while single-mutated viruses are settled in between. This implies a synergistic effect of both mutations for the earlier induction of $CD8^{+}$ T cells.

A similar picture is seen with the restimulation of memory T cells with respective viral epitopes. Again, P52 is significantly superior to WE in the frequency of GP33 and NP396 specific T cells able to produce IFNγ and TNFα after peptide stimulation. While the virus carrying the I181M mutation (P29-2.1) showed no difference, the number of T cells induced by R185W-mutated virus (P29-1.3) was increased comparably to those of P52. Together with the trend observed in the T cell kinetic, the mutation at position 185 in the viral glycoprotein seems to be important for the stronger T cell response by P52, but still position 181 is further enhancing this effect.

This observation is contrasting to the lower IFN-I levels found in serum at day 1 as IFN-I is important for activation of $CD8^+$ T cells (Kolumam et al., 2005). Here, the ambivalent role of an early infection of DCs might become visible. It usually results in a potent innate immune activation but goes hand in hand with an early destruction of DCs, limiting the adaptive immune response.

$CD169^+$ macrophages are also able to prime $CD8^+$ T cells in the absence of DCs (Bernhard et al., 2015). As LCMV-P52 shows a higher infection rate of $CD169^+$ macrophages in the splenic marginal zone, this might compensate the lower IFN-I levels and finally induce a more potent anti-viral T cell response.

During infection with P52, the balance of innate and adaptive response is slightly shifted towards adaptive immunity with lower IFN-I levels, but higher frequencies of anti-viral $CD8^+$ T cells. Lower IFN-I levels indicate less side effects, as high IFN-I is correlated with a higher disease score for other arenaviruses (Hickerson et al., 2020). The earlier and stronger $CD8^+$ T cell response ensures an efficient clearance of the virus. Concludingly, these aspects suggest a P52 to be a better tolerated therapy than the wildtype virus WE.

To complete the evaluation of adaptive responses, the induction of neutralizing antibodies was measured. This a widely used mechanism to finally control a viral infection by neutralizing the last remaining infectious particles. In contrast to many other viruses, several arenaviruses have glycosylations protecting the receptor-binding site of the glycoprotein from neutralizing antibodies. Thus, nAb against LCMV are rarely seen in C57BL/6 mice. As the two mutations do not affect the glycosylation motifs NXS or NXT (Sommerstein et al., 2015), no changes in the glycan shields are expected. Accordingly, no neutralizing antibodies were found in any of the viruses until day 30 after infection.

2.2.5 Immunopathology

LCMV-WE is used as a model of virus-induced hepatitis. The destruction of the hepatocytes is not induced by the virus itself but by T cell-mediated killing of infected hepatocytes. For an

increase in hepatic enzymes in serum, infection of hepatocytes and anti-viral T cells must come together. P52, although eliciting stronger T cell activation, showed significantly decreased levels of hepatic enzymes in serum indicating less infection of hepatocytes.

The reduced destruction of hepatocytes is a clear indicator for less side effects making P52 a better tool for treating cancer in patients.

2.2.6 Tumor Growth Inhibition

Viral penetration of the tumor tissue appears to be a critical aspect for LCMV viroimmunotherapy. The observed tropism shift with improved infection of tumor cells gives a first hint to a better treatment efficacy of P52 in tumor-bearing mice. As expected, the LCMV-WE and all mutant viruses were able to inhibit the growth of H1975 xenograft tumors in NOD.SCID mice, although the differences between the viruses were not significant. A possible explanation for this might be the immunodeficiency of the NOD.SCID mice as they are lacking functional T and B cells. Taking the phenotypical changes of P52 with less IFN-I but more $CD8^+$ T cells into account, the used model might cover the actual differences.

To overcome this limitation, the efficacy of P52 was investigated in an immunocompetent model. B16-Ova tumor-bearing C57BL/6 mice were treated with P52 in combination with an antibody blocking the PD-1 to enhance the T cell mediated effect against the tumor. PD-1 is a marker for T cell exhaustion that is upregulated in cases of prolonged antigen presence as seen in established tumors. The blocking of this immune checkpoint with an antibody is an effective therapy for many solid tumors and also often used as a combination partner for new immune stimulating agents.

Indeed, the combination of both treatments synergistically increased the efficacy while the PD-1 blockade alone had no significant impact on the tumor growth. This complies with the late onset of the regression starting from day 9, as this is the peak of anti-viral T cell response. As the B16-Ova cell line is usually resistant to PD-1 blockade, this observation suggests a second possible indication for P52 treatment, by “sensitizing” αPD-1-resistant tumors to the commonly used antibody therapy. A possible mechanism could be the attraction of $CD8^+$ T cells into the tumor tissue which is known to show only very low numbers of T cells that can profit from the checkpoint inhibition. This second pathway might even be working without direct effect of the virus treatment alone.

4.3 Possible Mode of Action

In contrast to oncolytic viruses, the LCMV is a non-cytopathic virus, which does not lyze infected tumor cells directly, but induces a strong anti-viral T cell response. This leads to a longer

persistence and better penetration of the entire tumor than replication-deficient viruses, leading to a prolonged cytokine production with consecutive infiltration of T cells and NK cells e.g., via C-C motif ligand 5 (CCL5) (H. Bhat et al., 2020).

Most of the T cells expanding during LCMV infection are virus-specific, but a certain bystander population is seen, which has no significant biological relevance for control of viral infection (Ehl et al., 1997). But infiltration of non-virus-specific T cells into inflamed tissue, in this special case the tumor, increases the chance for antigen recognition by tumor-specific T cells. Together with the cytokine milieu, e.g. IFN-I induced by the viral infection (Kalkavan et al., 2017), efficient priming and activation of neoantigen-recognizing T cells appears possible (Kim & Shin, 2019). This would induce an anti-tumoral response, lasting far longer than the viral persistence. Here, a single treatment can direct the hosts immune response towards malignant cells.

A similar observation was made with a mouse model for type I diabetes, where bystander T cells react against pancreatic β-cells (Pane & Coulson, 2015). Another study implies that already existing tumor-specific memory T cells are re-activated as bystander (Tietze et al., 2012).

Nevertheless, it must be considered that anti-tumoral T cells often exhaust due to the high antigen load especially in late stages of disease or because of PD-L1 expression by tumor cells. Therefore, checkpoint inhibitors blocking exhaustion pathways like PD-1 show great effects in clinical use. And indeed, the anti-tumoral effect of LCMV is even enhanced by combination with an αPD-1 antibody in the B16-Ova model, which is poorly responding to PD-1 blockade alone.

This clearly suggests a significant role of T cells but cannot explain the effects seen in T cell-deficient NOD.SCID mice. This implies a multi-modal immune activation including also innate pathways like IFN-I (Kalkavan et al., 2017) or CCL5-mediated NK cell infiltration (H. Bhat et al., 2020).

IFN-I is also known to upregulate MHC-I expression and antigen presentation (Fellous et al., 1982), again pointing at the potential role of $CD8^+$ T cells, implicating a functional role in anti-tumoral effect of arenaviruses (F. Zhou et al., 2019).

4.4 Limitations of this Work

This work demonstrates the possibility of changing a virus' phenotype by use of the new developed Fast Evolution Platform. The mutant virus P52 shows significant differences in T cell kinetics and tends to be more effective in treatment of human NSCLC xenograft model.

The improved T cell responses were only investigated in naïve, tumor-free mice. Effects of the presence of tumor cells need to be further elucidated, as the presence of B16-Ova tumors e.g. improves the proliferation of Ova-specific T cells after vaccination with LCMV-Ova, a replication-deficient LCMV expressing the Ova-antigen (F. Zhou et al., 2019). On the other hand, presence of an B16F10 tumor suppresses the anti-viral immune response via a yet unknown mechanism (Russ et al., 2011).

For a long-lasting anti-tumoral immune response, $CD8^+$ T cells recognizing tumor neoantigens are indispensable. Assessing the frequency and expansion of tumor-specific T cells would give a better understanding of the mechanism. Here, a possible way to examine activation and proliferation of tumor-specific T cells could be the transfer of OT-I T cells. The OT-I mice carry a transgenic TCR recognizing the $Ova_{257-264}$ epitope which is expressed by e.g., B16-Ova cells. Together with the use of congenic CD45.1 mice, differentiation between tumor-specific (OT-I, $CD45.2^+$) and host ($CD45.1^+$) T cells allows the detailed tracking and quantification of these tumor-specific cells.

Together with the fact that anti-tumoral effect is also seen in lymphocyte-deficient NOD.SCID mice, innate mechanisms have to play an important role. Although IFN-I was shown to be a major part in anti-tumoral behavior of LCMV-WE (Kalkavan et al., 2017), the serum IFNα was lower in the P52-treated group. As consequence, there have to be more innate pathways being activated in the tumor tissue, still leaving open questions in concern of mechanism of anti-tumoral effect.

4.5 Outlook

To allow the conclusion if the two occurred mutations significantly enhance anti-tumoral capacity of LCMV-WE, further investigation about the mode of action needs to be performed. For this, the use of different syngeneic tumor models in immune-competent mice is necessary, representing hot and cold tumor models, which differ in their immune infiltrates and cytokine milieu. An interesting aspect would be possible changes in the tumor microenvironment. Can a cold tumor be turned into a hot one? Is the virus treatment switching the suppressive microenvironment into an inflamed tumor tissue?

The newly established Fast Evolution Platform offers a great modular tool to find many different viruses that show advantageous properties like enhanced penetration of tumor tissue, stronger innate and adaptive immune activation, and lower side effects in healthy tissue in many different tumor entities. Here, the platform can be extended by more human or non-human cell lines, primary cells, or i*n vivo* passages with tumor-bearing mice to generate new mutations that show

other beneficial treats. Also, the addition of cytokines or special media or cultivation conditions can be easily integrated into the platform to mimic the tumor microenvironment. The combination of different replication-enhancing mutations with those that tend to reduce replication in healthy tissue could give a superior virotherpeutic agent to finally treat many forms of solid cancer without severe side-effects.

5. Conclusion

The diagnosis of an malignant cancer is always life-threatening and goes hand in hand with a long lasting therapy with many and partially severe side effects. To overcome this, the development of new therapeutic approaches is indispensible.

In the last decade, many live-attenuated viruses were tested with different success. Another approach with replication-competent virus was published to be effective in mice. Unfortunately, the used WE-strain of Lymphocytic Choriomeningitis Virus (LCMV) induced transient hepatitis in mice.

In this work, the wildtype virus WE was passaged on human cancer cells in order to shift the viral tropism from healthy cells towards malignant cells. And indeed, two mutations within the tropism-defining glycoprotein were found after 52 passages and characterized *in vitro* and *in vivo*.

The *in vitro* replication on different human tumor cell lines showed a clear pattern. The mutant virus, and to a certain level also the single-mutants carrying only one of the two mutations, yield higher virus titers in the supernatant at early timepoints, especially after infection with low doses of virus. This supports the hypothesis of changed tropism and higher binding affinity to tumor cells.

Infection of naïve mice with the mutated virus induced significantly stronger T cell response compared to WE. In contrast, the serum levels of alanine transaminase (ALT), aspartate transaminase (AST) and lactate dehydrogenase (LDH) that corelate with destruction of virus-infected hepatocytes by virus-specific T cells was reduced in all mutant virus infected mice indicating less infection of hepatocytes. This underlines the tropism change with less infection of healthy cells. Additionally, the peak values of type I interferon (IFN-I) was significantly reduced on day 1 in serum which might reduce the early side effects of the future therapy.

A beneficial role of mutated LCMV was also found in combination with blockade of programmed cell death 1 (PD-1), offering oppertunities for later combination treatments.

Considering the higher replication in tumor cells and decreased infection of healthy cells in combination with reduced side effects, the mutated virus is superior to the wildtype regarding its capacity as viroimmunotherapetic. This examples proofs the possibility to generate a virus with better anti-tumoral properties by simple and fast serial passages. This opens up the chance to further improve the virus or combine mutations to generate a well-working and safe virotherapeutic agent.

6. Literature

1. Andtbacka, R. H., Kaufman, H. L., Collichio, F., Amatruda, T., Senzer, N., Chesney, J., Delman, K. A., Spitler, L. E., Puzanov, I., Agarwala, S. S., Milhem, M., Cranmer, L., Curti, B., Lewis, K., Ross, M., Guthrie, T., Linette, G. P., Daniels, G. A., Harrington, K., Middleton, M. R., Miller, W. H., Jr., Zager, J. S., Ye, Y., Yao, B., Li, A., Doleman, S., VanderWalde, A., Gansert, J.,Coffin, R. S. (2015): Talimogene Laherparepvec improves durable response rate in patients with advanced melanoma. J Clin Oncol 33, 2780-2788.

2. Arstila, T. P., Casrouge, A., Baron, V., Even, J., Kanellopoulos, J.,Kourilsky, P. (1999): A direct estimate of the human alphabeta T cell receptor diversity. Science 286, 958-961.

3. Attaf, M., Huseby, E.,Sewell, A. K. (2015): αβ T cell receptors as predictors of health and disease. Cellular & Molecular Immunology 12, 391-399.

4. Barbalat, R., Lau, L., Locksley, R. M.,Barton, G. M. (2009): Toll-like receptor 2 on inflammatory monocytes induces type I interferon in response to viral but not bacterial ligands. Nat Immunol 10, 1200-1207.

5. Barzaghi, F., Passerini, L.,Bacchetta, R. (2012): Immune dysregulation, polyendocrinopathy, enteropathy, x-linked syndrome: a paradigm of immunodeficiency with autoimmunity. Front Immunol 3, 211.

6. Beier, J. I., Jokinen, J. D., Holz, G. E., Whang, P. S., Martin, A. M., Warner, N. L., Arteel, G. E.,Lukashevich, I. S. (2015): Novel mechanism of arenavirus-induced liver pathology. PloS one 10, e0122839-e0122839.

7. Bernhard, C. A., Ried, C., Kochanek, S.,Brocker, T. (2015): CD169+ macrophages are sufficient for priming of CTLs with specificities left out by cross-priming dendritic cells. Proceedings of the National Academy of Sciences 112, 5461-5466.

8. Bhat, H., Zaun, G., Hamdan, T. A., Lang, J., Adomati, T., Schmitz, R., Friedrich, S.-K., Bergerhausen, M., Cham, L. B., Li, F., Ali, M., Zhou, F., Khairnar, V., Duhan, V., Brandenburg, T., Machlah, Y. M., Schiller, M., Berry, A., Xu, H., Vollmer, J., Häussinger, D., Thier, B., Pandyra, A. A., Schadendorf, D., Paschen, A., Schuler, M., Lang, P. A.,Lang, K. S. (2020): Arenavirus induced CCL5 expression causes NK cell-mediated melanoma regression. Frontiers in Immunology 11

9. Bhat, K. H.,Yaseen, I. (2018). Mycobacterium tuberculosis: Macrophage takeover and modulation of innate effector responses. In: W. Ribón (Hrsg.): Mycobacterium. Rijeka: IntechOpen

10. Bonthius, D. J. (2012): Lymphocytic choriomeningitis virus: an underrecognized cause of neurologic disease in the fetus, child, and adult. Seminars in pediatric neurology 19, 89-95.

11. Broadley, Steven P., Plaumann, A., Coletti, R., Lehmann, C., Wanisch, A., Seidlmeier, A., Esser, K., Luo, S., Rämer, Patrick C., Massberg, S., Busch, Dirk H., van Lookeren Campagne, M.,Verschoor, A. (2016): Dual-track clearance of circulating bacteria balances rapid restoration of blood sterility with induction of adaptive immunity. Cell Host & Microbe 20, 36-48.

12. Cai, M., Li, M., Wang, K., Wang, S., Lu, Q., Yan, J., Mossman, K. L., Lin, R.,Zheng, C. (2013): The herpes simplex virus 1-encoded envelope glycoprotein B activates NF-κB through the Toll-like receptor 2 and MyD88/TRAF6-dependent signaling pathway. PloS one 8, e54586-e54586.

13. Cao, W., Henry, M. D., Borrow, P., Yamada, H., Elder, J. H., Ravkov, E. V., Nichol, S. T., Compans, R. W., Campbell, K. P.,Oldstone, M. B. (1998): Identification of alpha-dystroglycan as a receptor for lymphocytic choriomeningitis virus and Lassa fever virus. Science (New York, N.Y.) 282, 2079-2081.

14. Chaplin, D. D. (2010): Overview of the immune response. J Allergy Clin Immunol 125, S3-23.

15. Copelan, E. A. (2006): Hematopoietic stem-cell transplantation. N Engl J Med 354, 1813-1826.

16. Coyle, A. L. (2016): Lassa fever. Nursing2020 46

17. Cuevas, C. D.,Ross, S. R. (2014): Toll-like receptor 2-mediated innate immune responses against Junín virus in mice lead to antiviral adaptive immune responses during systemic infection and do not affect viral replication in the brain. Journal of virology 88, 7703-7714.

18. Daugan, M., Murira, A., Mindt, B. C., Germain, A., Tarrab, E., Lapierre, P., Fritz, J. H.,Lamarre, A. (2016): Type I interferon impairs specific antibody responses early during establishment of LCMV infection. Frontiers in immunology 7, 564-564.

19. Di Simone, C., Zandonatti, M. A.,Buchmeier, M. J. (1994): Acidic pH triggers LCMV membrane fusion activity and conformational change in the glycoprotein spike. Virology 198, 455-465.

20. Dixon, L. J., Barnes, M., Tang, H., Pritchard, M. T.,Nagy, L. E. (2013): Kupffer cells in the liver. Compr Physiol 3, 785-797.

21. Dranoff, G. (2004): Cytokines in cancer pathogenesis and cancer therapy. Nat Rev Cancer 4, 11-22.

22. Ehl, S., Hombach, J., Aichele, P., Hengartner, H.,Zinkernagel, R. M. (1997): Bystander activation of cytotoxic T cells: studies on the mechanism and evaluation of in vivo

significance in a transgenic mouse model. The Journal of experimental medicine 185, 1241-1251.

23. Eschli, B., Quirin, K., Wepf, A., Weber, J., Zinkernagel, R.,Hengartner, H. (2006): Identification of an N-terminal trimeric coiled-coil core within Arenavirus glycoprotein 2 permits assignment to class I viral fusion proteins. Journal of Virology 80, 5897.

24. Eto, A., Yamamoto, N.,Kanatani, Y. (2021): Effect of serial passage on the pathogenicity and immunogenicity of Vaccinia virus LC16m8 strain. Biology 10, 1158.

25. Fellous, M., Nir, U., Wallach, D., Merlin, G., Rubinstein, M.,Revel, M. (1982): Interferon-dependent induction of mRNA for the major histocompatibility antigens in human fibroblasts and lymphoblastoid cells. Proceedings of the National Academy of Sciences of the United States of America 79, 3082-3086.

26. Flatz, L., Hegazy, A. N., Bergthaler, A., Verschoor, A., Claus, C., Fernandez, M., Gattinoni, L., Johnson, S., Kreppel, F., Kochanek, S., Broek, M. v. d., Radbruch, A., Lévy, F., Lambert, P.-H., Siegrist, C.-A., Restifo, N. P., Löhning, M., Ochsenbein, A. F., Nabel, G. J.,Pinschewer, D. D. (2010): Development of replication-defective lymphocytic choriomeningitis virus vectors for the induction of potent CD8+ T cell immunity. Nature medicine 16, 339-345.

27. Friedrich, S. K., Schmitz, R., Bergerhausen, M., Lang, J., Cham, L. B., Duhan, V., Häussinger, D., Hardt, C., Addo, M., Prinz, M., Asano, K., Lang, P. A.,Lang, K. S. (2020): Usp18 expression in CD169(+) macrophages is important for strong immune response after vaccination with VSV-EBOV. Vaccines (Basel) 8

28. Hallam, S. J., Koma, T., Maruyama, J.,Paessler, S. (2018): Review of Mammarenavirus biology and replication. Frontiers in microbiology 9, 1751-1751.

29. Hastie, K. M., Igonet, S., Sullivan, B. M., Legrand, P., Zandonatti, M. A., Robinson, J. E., Garry, R. F., Rey, F. A., Oldstone, M. B.,Saphire, E. O. (2016): Crystal structure of the prefusion surface glycoprotein of the prototypic arenavirus LCMV. Nature structural & molecular biology 23, 513-521.

30. Hastie, K. M., Zandonatti, M. A., Kleinfelter, L. M., Heinrich, M. L., Rowland, M. M., Chandran, K., Branco, L. M., Robinson, J. E., Garry, R. F.,Saphire, E. O. (2017): Structural basis for antibody-mediated neutralization of Lassa virus. Science 356, 923.

31. Hayes, M. W., Carrion, R., Jr., Nunneley, J., Medvedev, A. E., Salvato, M. S.,Lukashevich, I. S. (2012): Pathogenic Old World arenaviruses inhibit TLR2/Mal-dependent proinflammatory cytokines in vitro. J Virol 86, 7216-7226.

32. Hickerson, B. T., Sefing, E. J., Bailey, K. W., Van Wettere, A. J., Penichet, M. L.,Gowen, B. B. (2020): Type I interferon underlies severe disease associated with Junín virus infection in mice. eLife 9, e55352.

33. Hofmann, F.,Kralj, N. (2009): Criteria for successful hepatitis B vaccination in adults: results of a case study. Infection 37, 266-269.

34. Honke, N., Shaabani, N., Cadeddu, G., Sorg, U. R., Zhang, D. E., Trilling, M., Klingel, K., Sauter, M., Kandolf, R., Gailus, N., van Rooijen, N., Burkart, C., Baldus, S. E., Grusdat, M., Löhning, M., Hengel, H., Pfeffer, K., Tanaka, M., Häussinger, D., Recher, M., Lang, P. A.,Lang, K. S. (2011): Enforced viral replication activates adaptive immunity and is essential for the control of a cytopathic virus. Nat Immunol 13, 51-57.

35. Honke, N., Shaabani, N., Teijaro, J. R., Christen, U., Hardt, C., Bezgovsek, J., Lang, P. A.,Lang, K. S. (2017): Presentation of autoantigen in peripheral lymph nodes is sufficient for priming autoreactive CD8(+) T cells. Front Immunol 8, 113.

36. Jung, A., Kato, H., Kumagai, Y., Kumar, H., Kawai, T., Takeuchi, O.,Akira, S. (2008): Lymphocytoid choriomeningitis virus activates plasmacytoid dendritic cells and induces a cytotoxic T-cell response via MyD88. J Virol 82, 196-206.

37. Kalkavan, H., Sharma, P., Kasper, S., Helfrich, I., Pandyra, A. A., Gassa, A., Virchow, I., Flatz, L., Brandenburg, T., Namineni, S., Heikenwalder, M., Höchst, B., Knolle, P. A., Wollmann, G., von Laer, D., Drexler, I., Rathbun, J., Cannon, P. M., Scheu, S., Bauer, J., Chauhan, J., Häussinger, D., Willimsky, G., Löhning, M., Schadendorf, D., Brandau, S., Schuler, M., Lang, P. A.,Lang, K. S. (2017): Spatiotemporally restricted arenavirus replication induces immune surveillance and type I interferon-dependent tumour regression. Nature Communications 8, 14447.

38. Kallert, S. M., Darbre, S., Bonilla, W. V., Kreutzfeldt, M., Page, N., Müller, P., Kreuzaler, M., Lu, M., Favre, S., Kreppel, F., Löhning, M., Luther, S. A., Zippelius, A., Merkler, D.,Pinschewer, D. D. (2017): Replicating viral vector platform exploits alarmin signals for potent CD8(+) T cell-mediated tumour immunotherapy. Nat Commun 8, 15327.

39. Kim, T.-S.,Shin, E.-C. (2019): The activation of bystander CD8+ T cells and their roles in viral infection. Experimental & Molecular Medicine 51, 1-9.

40. Kolumam, G. A., Thomas, S., Thompson, L. J., Sprent, J.,Murali-Krishna, K. (2005): Type I interferons act directly on CD8 T cells to allow clonal expansion and memory formation in response to viral infection. The Journal of experimental medicine 202, 637-650.

41. Kunz, S., Edelmann, K. H., de la Torre, J.-C., Gorney, R.,Oldstone, M. B. A. (2003): Mechanisms for lymphocytic choriomeningitis virus glycoprotein cleavage, transport, and incorporation into virions. Virology 314, 168-178.

42. Kunz, S., Sevilla, N., Rojek, J. M.,Oldstone, M. B. A. (2004): Use of alternative receptors different than α-dystroglycan by selected isolates of lymphocytic choriomeningitis virus. Virology 325, 432-445.

43. Lapošová, K., Pastoreková, S.,Tomášková, J. (2013): Lymphocytic choriomeningitis virus: invisible but not innocent. Acta Virol 57, 160-170.

44. Liu, Y. T.,Sun, Z. J. (2021): Turning cold tumors into hot tumors by improving T-cell infiltration. Theranostics 11, 5365-5386.

45. Macneil, A., Ströher, U., Farnon, E., Campbell, S., Cannon, D., Paddock, C. D., Drew, C. P., Kuehnert, M., Knust, B., Gruenenfelder, R., Zaki, S. R., Rollin, P. E., Nichol, S. T.,Team, L. T. I. (2012): Solid organ transplant-associated lymphocytic choriomeningitis, United States, 2011. Emerging infectious diseases 18, 1256-1262.

46. Madera, S., Rapp, M., Firth, M. A., Beilke, J. N., Lanier, L. L.,Sun, J. C. (2016): Type I IFN promotes NK cell expansion during viral infection by protecting NK cells against fratricide. The Journal of experimental medicine 213, 225-233.

47. Martínez-Sobrido, L., Zúñiga, E. I., Rosario, D., García-Sastre, A.,de la Torre, J. C. (2006): Inhibition of the type I interferon response by the nucleoprotein of the prototypic arenavirus lymphocytic choriomeningitis virus. J Virol 80, 9192-9199.

48. Masopust, D., Murali-Krishna, K.,Ahmed, R. (2007): Quantitating the magnitude of the lymphocytic choriomeningitis virus-specific CD8 T-cell response: it is even bigger than we thought. Journal of virology 81, 2002-2011.

49. Mayr, A., Hochstein-Mintzel, V.,Stickl, H. (1975): Abstammung, Eigenschaften und Verwendung des attenuierten Vaccinia-Stammes MVA. Infection 3, 6-14.

50. McGavern, D. B.,Truong, P. (2004): Rebuilding an immune-mediated central nervous system disease: weighing the pathogenicity of antigen-specific versus bystander T cells. Journal of immunology (Baltimore, Md. : 1950) 173, 4779-4790.

51. McLay, L., Liang, Y.,Ly, H. (2014): Comparative analysis of disease pathogenesis and molecular mechanisms of New World and Old World arenavirus infections. The Journal of general virology 95, 1-15.

52. Mosely, S. I., Prime, J. E., Sainson, R. C., Koopmann, J. O., Wang, D. Y., Greenawalt, D. M., Ahdesmaki, M. J., Leyland, R., Mullins, S., Pacelli, L., Marcus, D., Anderton, J., Watkins, A., Coates Ulrichsen, J., Brohawn, P., Higgs, B. W., McCourt, M., Jones, H., Harper, J. A., Morrow, M., Valge-Archer, V., Stewart, R., Dovedi, S. J.,Wilkinson, R. W. (2017): Rational selection of syngeneic preclinical tumor models for immunotherapeutic drug discovery. Cancer Immunol Res 5, 29-41.

53. Moskophidis, D., Moskophidis, M.,Löhler, J. (1997): Virus-specific IgD in acute viral infection of mice. J Immunol 158, 1254-1261.

54. Muik, A., Stubbert, L. J., Jahedi, R. Z., Geiβ, Y., Kimpel, J., Dold, C., Tober, R., Volk, A., Klein, S., Dietrich, U., Yadollahi, B., Falls, T., Miletic, H., Stojdl, D., Bell, J. C.,von Laer, D. (2014): Re-engineering Vesicular stomatitis virus to abrogate neurotoxicity, circumvent humoral immunity, and enhance oncolytic potency. Cancer Research 74, 3567.

55. Norris, B. A., Uebelhoer, L. S., Nakaya, H. I., Price, A. A., Grakoui, A.,Pulendran, B. (2013): Chronic but not acute virus infection induces sustained expansion of myeloid suppressor cell numbers that inhibit viral-specific T cell immunity. Immunity 38, 309-321.

56. Pane, J. A.,Coulson, B. S. (2015): Lessons from the mouse: potential contribution of bystander lymphocyte activation by viruses to human type 1 diabetes. Diabetologia 58, 1149-1159.

57. Peters, C. J. (2006): Lymphocytic choriomeningitis virus--an old enemy up to new tricks. N Engl J Med 354, 2208-2211.

58. Recher, M., Lang, K. S., Hunziker, L., Freigang, S., Eschli, B., Harris, N. L., Navarini, A., Senn, B. M., Fink, K., Lötscher, M., Hangartner, L., Zellweger, R., Hersberger, M., Theocharides, A., Hengartner, H.,Zinkernagel, R. M. (2004): Deliberate removal of T cell help improves virus-neutralizing antibody production. Nature Immunology 5, 934-942.

59. Richter, K.,Oxenius, A. (2013): Non-neutralizing antibodies protect from chronic LCMV infection independently of activating FcγR or complement. European Journal of Immunology 43, 2349-2360.

60. Robert, C. (2020): A decade of immune-checkpoint inhibitors in cancer therapy. Nature Communications 11, 3801.

61. Russ, A. J., Xu, K., Wentworth, L., Alam, S., Meyers, J. V., Macklin, M. D., Rakhmilevich, A. L., Rajamanickam, V., Suresh, M.,Cho, C. S. (2011): Melanoma-induced suppression of tumor antigen-specific T cell expansion is comparable to suppression of global T cell expansion. Cell Immunol 271, 104-109.

62. Salvato, M., Clegg, J. C. S., Buchmeier, M., Charrel, R., Gonzalez, J.-P., Lukashevich, I., Peters, C.,Romanowski, V. (2011). Arenaviridae S. 715-723

63. Schwendinger, M., Thiry, G., De Vos, B., Leroux-Roels, G., Bruhwyler, J., Huygens, A., Ganeff, C., Buchinger, H., Orlinger, K. K., Pinschewer, D. D., Monath, T. P.,Lilja, A. E. (2020): A randomized dose-escalating phase I trial of a replication-deficient Lymphocytic choriomeningitis virus vector-based vaccine against human Cytomegalovirus. J Infect Dis

64. Sevilla, N., Domingo, E.,de la Torre, J. C. (2002): Contribution of LCMV towards deciphering biology of quasispecies in vivo. Current topics in microbiology and immunology 263, 197-220.

65. Shimojima, M., Ströher, U., Ebihara, H., Feldmann, H.,Kawaoka, Y. (2012): Identification of cell surface molecules involved in dystroglycan-independent Lassa virus cell entry. Journal of virology 86, 2067-2078.

66. Sleijfer, S., Bannink, M., Van Gool, A. R., Kruit, W. H.,Stoter, G. (2005): Side effects of interferon-alpha therapy. Pharm World Sci 27, 423-431.

67. Smelt, S. C., Borrow, P., Kunz, S., Cao, W., Tishon, A., Lewicki, H., Campbell, K. P.,Oldstone, M. B. (2001): Differences in affinity of binding of lymphocytic choriomeningitis virus strains to the cellular receptor alpha-dystroglycan correlate with viral tropism and disease kinetics. J Virol 75, 448-457.

68. Smith, K. A. (2012): Louis pasteur, the father of immunology? Frontiers in immunology 3, 68-68.

69. Sommerstein, R., Flatz, L., Remy, M. M., Malinge, P., Magistrelli, G., Fischer, N., Sahin, M., Bergthaler, A., Igonet, S., Ter Meulen, J., Rigo, D., Meda, P., Rabah, N., Coutard, B., Bowden, T. A., Lambert, P.-H., Siegrist, C.-A.,Pinschewer, D. D. (2015): Arenavirus glycan shield promotes neutralizing antibody evasion and protracted infection. PLoS pathogens 11, e1005276-e1005276.

70. Stamm, A., Valentine, L., Potts, R.,Premenko-Lanier, M. (2012): An intermediate dose of LCMV clone 13 causes prolonged morbidity that is maintained by CD4+ T cells. Virology 425, 122-132.

71. Stark, G. R., Kerr, I. M., Williams, B. R. G., Silverman, R. H.,Schreiber, R. D. (1998): How cells respond to interferons. Annual Review of Biochemistry 67, 227-264.

72. Straub, T., Schweier, O., Bruns, M., Nimmerjahn, F., Waisman, A.,Pircher, H. (2013): Nucleoprotein-specific nonneutralizing antibodies speed up LCMV elimination independently of complement and FcγR. European Journal of Immunology 43, 2338-2348.

73. Suprunenko, T.,Hofer, M. J. (2019): Complexities of type I interferon biology: Lessons from LCMV. Viruses 11, 172.

74. Tietze, J. K., Wilkins, D. E. C., Sckisel, G. D., Bouchlaka, M. N., Alderson, K. L., Weiss, J. M., Ames, E., Bruhn, K. W., Craft, N., Wiltrout, R. H., Longo, D. L., Lanier, L. L., Blazar, B. R., Redelman, D.,Murphy, W. J. (2012): Delineation of antigen-specific and antigen-nonspecific CD8(+) memory T-cell responses after cytokine-based cancer immunotherapy. Blood 119, 3073-3083.

75. van Boxel-Dezaire, A. H. H., Rani, M. R. S.,Stark, G. R. (2006): Complex modulation of cell type-specific signaling in response to type I interferons. Immunity 25, 361-372.

76. Weidmann, M., Sall, A. A., Manuguerra, J.-C., Koivogui, L., Adjami, A., Traoré, F. F., Hedlund, K.-O., Lindegren, G.,Mirazimi, A. (2011): Quantitative analysis of particles, genomes and infectious particles in supernatants of haemorrhagic fever virus cell cultures. Virology journal 8, 81-81.

77. Whitehead, S. S., Juhasz, K., Firestone, C. Y., Collins, P. L.,Murphy, B. R. (1998): Recombinant respiratory syncytial virus (RSV) bearing a set of mutations from cold-passaged RSV is attenuated in chimpanzees. J Virol 72, 4467-4471.

78. Zapata, J. C.,Salvato, M. S. (2013): Arenavirus variations due to host-specific adaptation. Viruses 5, 241-278.

79. Zeng, Z., Surewaard, Bas G. J., Wong, Connie H. Y., Geoghegan, Joan A., Jenne, Craig N.,Kubes, P. (2016): CRIg functions as a macrophage pattern recognition receptor to directly bind and capture blood-borne gram-positive bacteria. Cell Host & Microbe 20, 99-106.

80. Zhou, F., Kardash, J., Bhat, H., Duhan, V., Friedrich, S.-K., Bezgovsek, J., Kalkavan, H., Bergerhausen, M., Schiller, M., Machlah, Y., Brandenburg, T., Hardt, C., Krolik, M., Flatz, L., Lang, P. A.,Lang, K. S. (2019): Viral infection overcomes ineffectiveness of anti-tumoral CD8+ T cell mediated cytotoxicity. bioRxiv, 591198.

81. Zhou, S., Cerny, A. M., Zacharia, A., Fitzgerald, K. A., Kurt-Jones, E. A.,Finberg, R. W. (2010): Induction and inhibition of type I interferon responses by distinct components of lymphocytic choriomeningitis virus. J Virol 84, 9452-9462.

82. Zhou, S., Halle, A., Kurt-Jones, E. A., Cerny, A. M., Porpiglia, E., Rogers, M., Golenbock, D. T.,Finberg, R. W. (2008): Lymphocytic choriomeningitis virus (LCMV) infection of CNS glial cells results in TLR2-MyD88/Mal-dependent inflammatory responses. J Neuroimmunol 194, 70-82.

83. Zhou, S., Kurt-Jones, E. A., Mandell, L., Cerny, A., Chan, M., Golenbock, D. T.,Finberg, R. W. (2005): MyD88 is critical for the development of innate and adaptive immunity during acute lymphocytic choriomeningitis virus infection. Eur J Immunol 35, 822-830.

84. Zhou, X., Ramachandran, S., Mann, M.,Popkin, D. L. (2012): Role of lymphocytic choriomeningitis virus (LCMV) in understanding viral immunology: past, present and future. Viruses 4, 2650-2669.

85. Ziegler, C. M., Eisenhauer, P., Bruce, E. A., Weir, M. E., King, B. R., Klaus, J. P., Krementsov, D. N., Shirley, D. J., Ballif, B. A.,Botten, J. (2016): The Lymphocytic

choriomeningitis virus matrix protein PPXY late domain drives the production of defective interfering particles. PLoS pathogens 12, e1005501-e1005501.

86. Zinkernagel, R. M., Haenseler, E., Leist, T., Cerny, A., Hengartner, H.,Althage, A. (1986): T cell-mediated hepatitis in mice infected with lymphocytic choriomeningitis virus. Liver cell destruction by H-2 class I-restricted virus-specific cytotoxic T cells as a physiological correlate of the 51Cr-release assay? The Journal of experimental medicine 164, 1075-1092.

7. Appendix

7.1 List of Figures

Figure 1: LCMV structure.. 7
Figure 2: Viral entry.. 8
Figure 3: Genome replication and gene transcription 9
Figure 4: Cells of the immune system.. 10
Figure 5: Titration Scheme. 28
Figure 6: PCR of genomic subsegments 31
Figure 7: Viral titers of indicated passage number 40
Figure 8: Sequence alignment of WE and P52 of the coding sequence for amino acids 180 - 186 of viral glycoprotein. 41
Figure 9: Viral titer of indicated passage numbers 41
Figure 10: Crystal structure of LCMV GP. 42
Figure 11: Structure of LASV GP, bound by neutralizing antibodies 42
Figure 12: LCMV GP. Side and top view of estimated LCVM GP trimer 43
Figure 13: Example for double peak, indicating quasi species. 43
Figure 14: Sequence alignment of earlier passages 44
Figure 15: Sequence alignment of P29 subclones. 45
Figure 16: Replication capability in vitro 46
Figure 17: Virus titers in spleen 47
Figure 18: Immunofluorescent staining of spleen sections. 48
Figure 19: Organ titers on day 30 49
Figure 20: Serum IFNα levels at indicated time points 50
Figure 21: WE and P52 do not induce cytokine expression in BMDM via TLR2 51
Figure 22: P52 elicits a faster T cell response with higher frequencies on day 8 and 10 52
Figure 23: Restimulation of splenocytes on day 30 53
Figure 24: Total neutralizing Ig. 54
Figure 25: Activity of hepatic enzymes in the serum 55
Figure 26: Growth of H1975 tumors. 56
Figure 27: Tumor growth of B16-Ova tumors after treatment with P52 and αPD-1 57

7.2 List of Tables

Table 1: Materials used for cell culture 21
Table 2: Self-made buffers 21
Table 3: Reagents for cell and mouse work 22
Table 4: Reagents for RNA and sequencing 22
Table 5: Antibodies 23
Table 6: cell lines 23
Table 7: single-use materials 24
Table 8: Primers 24
Table 9: PCR Settings 31
Table 10: devices 39
Table 11: manual tools 39

7.3 Abbreviations

Ab	Antibody
α-DG	α-Dystroglycan
ALAT	Alanine aminotransferase
APC	Allophycocyanin
ASAT	Aspartate aminotransferase
ATCC	American Type Culture Collection
B-ME	B-mercaptoethanol
BCR	B cell receptor
BMDM	Bone marrow-derived macrophage
BSC	Biosafety cabinet
CCL5	C-C motif ligand 5
CD	Cluster of Differentiation
cDC	Conventional Dendritic cell
cDNA	Complementary DNA
CGM	Complete growth medium
CNS	Central nervous system
CSF2	Colony-stimulating factor 2
CT	Threshold cycle
CTL	Cytotoxic T lymphocyte
CTLA-4	Cytotoxic T lymphocyte antigen 4
DC	Dendritic cell
DC-SIGN	Dendritic cell-specific intercellular adhesion molecule-3-grabbing non-integrin
DMEM	Dulbecco's modified Eagle's medium
DMSO	Dimethyl sulfoxide
DNA	Deoxyribonucleic acid
dNTP	Deoxynucleoside triphosphate
DTT	Dithiothreitol
ECM	Extracellular matrix
EDTA	Ethylenediaminetetraacetic acid
eIF2α	Eukaryotic translation initiation factor 2, α-subunit
ELISA	Enzyme-linked immunosorbent assay
ER	Endoplasmic reticulum
ES	Embryonic stem
FACS	Fluorescence-activated cell sorting
FCS	Fetal calf serum
FEP	Fast Evolution Platform
FoxP3	Forkhead box protein P3
GM-CSF	Granulocyte-macrophage colony-stimulating factor
GP1	Glycoprotein 1
GP2	Glycoprotein 2
GPc	Glycoprotein complex
GP-TET	GP33-loaded Tetramer
HLA	Human leukocyte antigen
HRP	Horseradish peroxidase
HSV-1	Herpes simplex virus 1
I	Isoleucine

ICP34.5	Infected cell protein 34.5
ICP47	Infected cell protein 47
ICS	Intracellular cytokine staining
IFNα	Interferon α
IFNα4	Interferon α4
Ifnar	Interferon α receptor
IFNβ	Interferon β
IFNγ	Interferon γ
IFN-I	Type I interferon
Ig	Immunoglobulin
IGR	Intergenic region
IL-10	Interleukin 10
IL-13	Interleukin 13
IL-4	Interleukin 4
IL-6	Interleukin 6
IPEX	Immunodysregulation polyendocrinopathy enteropathy X-linked
IRF	Interferon regulatory factor
ISG	Interferon-stimulated gene
JAK	Janus kinase
LSECtin	Lymph node sinusoidal endothelium calcium-dependent lectin
JUNV	Junín virus
Lanuv	Landesamt für Natur, Umwelt und Verbraucherschutz
LASV	Lassa virus
LCMV	Lymphocytic choriomeningitis virus
LDH	Lactate dehydrogenase
LTA	Lipoteichoic acid
M	methionine
MAVS	Mitochondrial antiviral-signaling protein
MCP-1	Monocyte chemotactic protein 1
M-CSF	Macrophage colony-stimulating factor
MDA5	Melanoma differentiation-associated protein 5
MHC	Major histocompatibility complex
MHC-I	Major histocompatibility complex class I
MHC-II	Major histocompatibility complex class II
MOI	Multiplicity of infection
MVA	Modified Vaccinia Ankara
MyD88	Myeloid differentiation primary response 88
MZ	Marginal zone
nAb	Neutralizing Antibody
NF-κB	Nuclear factor kappa-light-chain-enhancer of activated B cells
NK	Natural killer
NP	Nucleoprotein
NSCLC	Non-Small Cell Lung Cancer
OPD	o-Phenylenediamine
ORF	Open reading frame
Ova	Ovalbumin
PAMP	Pathogen-associated molecular pattern
PBS	Phosphate buffered saline

PCR	Polymerase chain reaction
PD-1	Programmed cell death protein 1
pDC	Plasmocytic Dendritic cell
PD-L1	Programmed cell death ligand 1
PE	Phycoerythrin
PE-Cy7	Phycoerythrin-Cyanine 7
FFU	Focus-forming unit
Prkdc	protein kinase, DNA-activated, catalytic subunit
R	Arginine
PRR	Pattern recognition receptor
qPCR	Quantitative Polymerase chain reaction
RBC	Red blood cell
RIG-I	Retinoic acid inducible gene I
RNA	Ribonucleic acid
RNP	Ribonucleoprotein
RPMI	Roswell Park Memorial Institute
RT	Reverse transcription
S1P	Site 1 protease
SSP	Stable signaling peptide
TCR	T cell receptor
TET	Tetramer
TLR	Toll-like receptor
TLR2	Toll-like receptor 2
TLR3	Toll-like receptor 3
TLR2/6	Dimer of Toll-like receptor 2 and 6
TLR7	Toll-like receptor 7
TLR8	Toll-like receptor 8
TNFα	Tumor necrosis factor α
TRIF	TIR domain-containing adaptor-inducing interferon-β
Usp18	Ubiquitin specific protease 18
UTR	Untranslated region
UV	Ultraviolet
VLE	Very low endotoxin
VSV	Vesicular stomatitis virus
VSV-G	Vesicular stomatitis virus glycoprotein
VSV-GP	VSV, carrying LCMV-GP
W	Tryptophan
WT	Wildtype

8. Lebenslauf

Der Lebenslauf ist in der Online-Version aus Gründen des Datenschutzes nicht enthalten.